FINAL REPORT JPL CONTRACT NO. 95080

[redacted]

HES

[redacted]

HUGHES RESEARCH LABORATORIES • MALIBU

HUGHES RESEARCH LABORATORIES
Malibu, California

a division of hughes aircraft company

INVESTIGATION OF THE DC-EXCITED XENON LASER

Final Report
24 March 1964 through 24 March 1965

JPL Contract No. 950803

Peter O. Clark, Richard A. Hubach,
and James Y. Wada

This work was performed for the Jet Propulsion Laboratory, California Institute of Technology, sponsored by the National Aeronautics and Space Administration under Contract NAS7-100.

BLANK PAGE

TABLE OF CONTENTS

LIST OF ILLUSTRATIONS

BLANK PAGE

I. INTRODUCTION

The purpose of this program was to investigate the development of a high power infrared gas laser, particularly the xenon laser. Several approaches were taken. Information regarding basic processes in the xenon discharge was obtained as a result of detailed measurements of optical gain and through extensive spectroscopic investigations of both spontaneous and stimulated infrared emission. Several new discharge configurations were designed with a view toward obtaining higher output power through the selective excitation of upper laser levels by controlled electron distributions. In addition, an investigation of the electron energy distribution in a dc-excited xenon plasma was performed using the Heil electron spectrometer.

Section II of this report is a detailed summary of the experiments performed to measure optical gain in a dc-excited xenon discharge at 3.5080 μ. The results of spectroscopic measurements of spontaneous and stimulated emission in the 0.9 to 13.0 μ wavelength region are presented in Section III. A tentative explanation of competing processes in the laser discharge based on these spectroscopic measurements is included. Section IV is a description of the pulsed xenon laser oscillating at wavelengths in the 1 to 9 μ interval.

A summary of experiments with several new discharge configurations is given in Section V. These new laser designs include a cold hollow cathode discharge, two heated hollow cathode discharges, and a multigrid or pentode configuration. Section VI is a description of the measurement of electron energy spectra in gas laser discharges. A summary of results and conclusions comprises Section VII of this report.

BLANK PAGE

II. MEASUREMENT OF OPTICAL GAIN AT 3.508 μ

A. Introduction

The objective of this portion of the program was to determine the effect of gas pressure and tube diameter on the operating characteristics of a pure xenon dc-excited amplifier. These measurements were obtained as curves and approximate relationships among the parameters. They are useful for the design of xenon amplifiers and oscillators which must satisfy specified requirements on optical gain and output power at 3.508 μ, and they provide some insight into the factors which limit these quantities.

Limited measurements of high, small-signal optical gain at 3.508 μ in pure dc-excited discharges were made previously,[1,2] and preliminary observations have indicated an improvement of 16 dB in minimum detectable signal and a spontaneous emission output of 4×10^{-9} W/noise mode.[3] The present measurements extend the results of the earlier investigations.

Large amplification has been observed in helium-xenon.[4] However, dc discharges in noble gas mixtures demonstrate strong cataphoresis which causes some difficulty in obtaining uniform, long-term operation. Another reason for restricting the present measurements to pure xenon is that although the addition of helium may increase the gain somewhat, the greater power required for the discharge leads to a net decrease in operating efficiency.

B. Experimental Apparatus

The experimental apparatus for the measurement of optical gain at 3.508 μ is illustrated schematically in Fig. 1. This is a phase locked detection system which is able to discriminate between the amplified signal and the spontaneous emission in the amplifier at low signal levels and under conditions which result in low amplifier gain. The signal source used in these measurements was a superradiant laser, i.e., a high gain laser with only one mirror. The major contribution to the output from such a source results from the noise generated in the end of the discharge which is farthest from the mirror. This noise is then amplified by two passes through the length of the tube. The signal level of the source was sufficiently high that aperture A_1 could be made small enough that noise from the near end of the amplifier made a negligible contribution to the superradiant output. This was checked by placing a very thin tilted quartz flat between the amplifier and source and to the right of aperture A_1. The signals reflected from the quartz flat were compared under amplifier on and amplifier off conditions. With no attenuators in place, the contribution

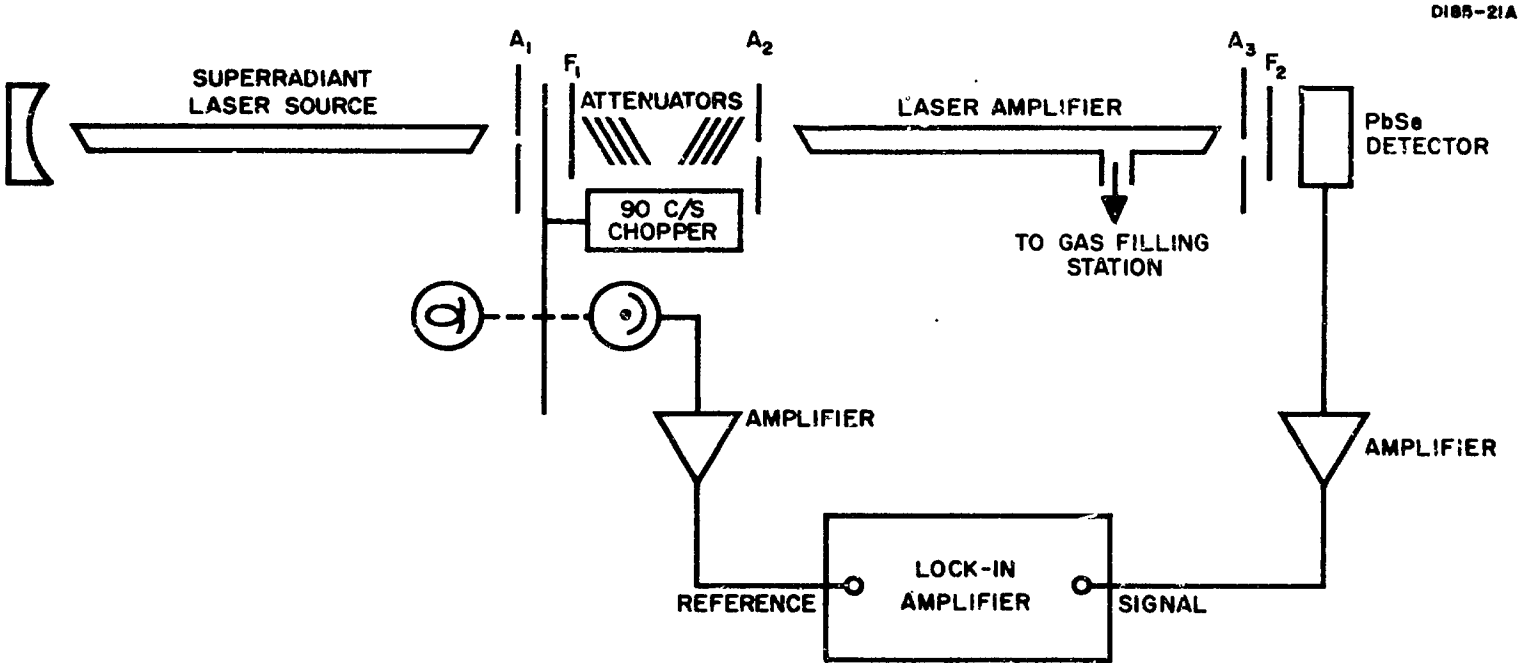

Fig. 1. Experimental system to measure amplification in xenon.

of the amplifier noise to the superradiant output was less than 5%. The output frequency of the superradiant source is fixed at the center of the Doppler-broadened line, and the line width is less than the Doppler width; the degree of narrowing depends upon the double-pass amplification of the laser source. It is felt that the error introduced by the non-negligible spectral width of the superradiant source is less serious than the measurement inaccuracies resulting from amplitude and frequency instabilities in a conventional laser oscillator.

F_1 and F_2 were multilayer filters centered at 3.508 μ with bandwidths of 0.1 μ. F_1 was tilted slightly to prevent possible laser oscillation between the aluminized spherical mirror and F_1. The attenuators were glass filters (Corning 7-56) which were inclined slightly to prevent reflected light from returning to either the superradiant source or the amplifier. They had previously been calibrated at 3.508 μ with an Eppley thermopile and were found to have attenuations ranging from 5.2 to 5.8 dB. When making the amplification measurements, the attenuators were used in oppositely tilted pairs whenever possible in order to eliminate refraction effects and maintain a constant propagation direction through the amplifier. Aperture A_2 was used to limit the beam size incident on the amplifier to prevent multiple paths by reflection from the inner walls of the tube. Aperture A_3 shielded the detectors from the hot cathode of the amplifier laser but was not small enough to intercept the beam. In addition, all surfaces which might cause specular back-reflections into either the source or the amplifier were roughened and blackened in order to minimize this effect.

The amplifiers were hot cathode dc-excited discharges with amplification path lengths of 50 cm. A typical discharge tube is shown in Fig. 2. Three tubes with bore diameters of 8, 5.1, and 2.6 mm were tested. During the measurements each tube remained connected to the gas filling and vacuum station. The xenon pressure was varied from 150 to 10 mTorr. At lower pressures, rapid cleanup of the xenon prevented reliable measurements. Alignment and transmission through the amplifier were checked by measuring the unattenuated signal power at a point between the amplifier and aperture A_2 (with filter F_2 placed directly behind A_2 for this measurement only) and at another point to the right of filter F_2. These measurements were made with the Eppley thermopile which has a sufficiently large aperture to measure total power. The measured transmission was approximately 0.85; this agrees well with a value of 0.88 for two Brewster angle quartz windows calculated from published data.

A three-vane chopper was used to modulate the signal at approximately 90 cps. A light source and photocell were included inside the chopper housing to provide a reference signal for the lock-in amplifier (Princeton Applied Research Model JB-5). The detector was a lead

M 3890

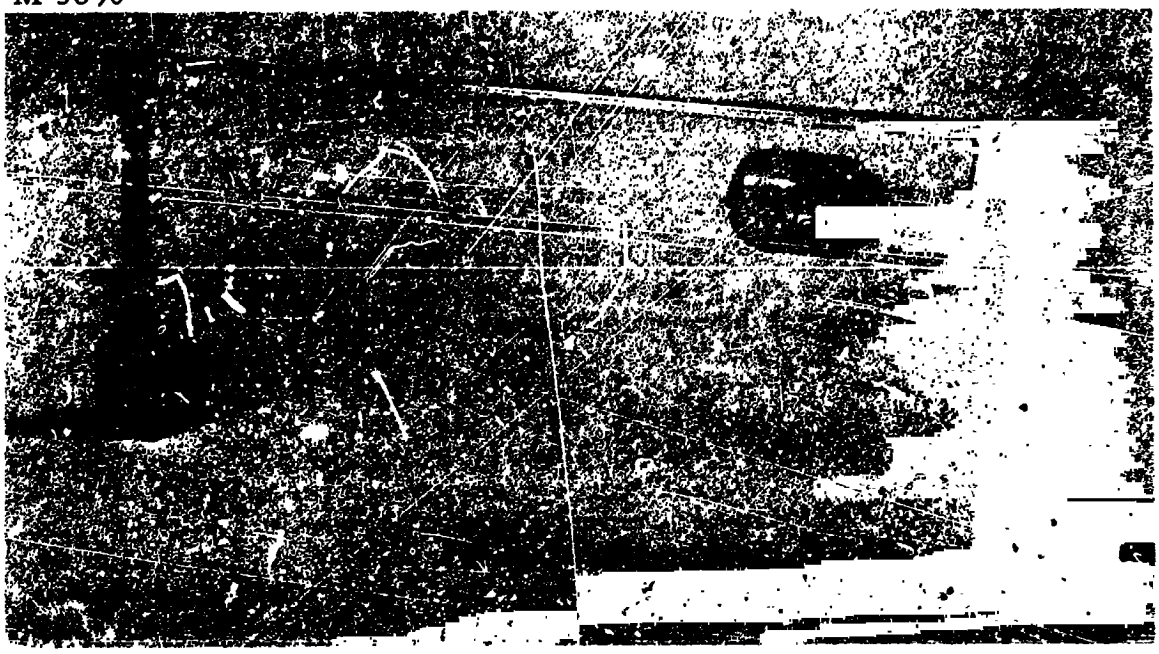

Fig. 2. Typical xenon amplifier used in the amplification measurements.

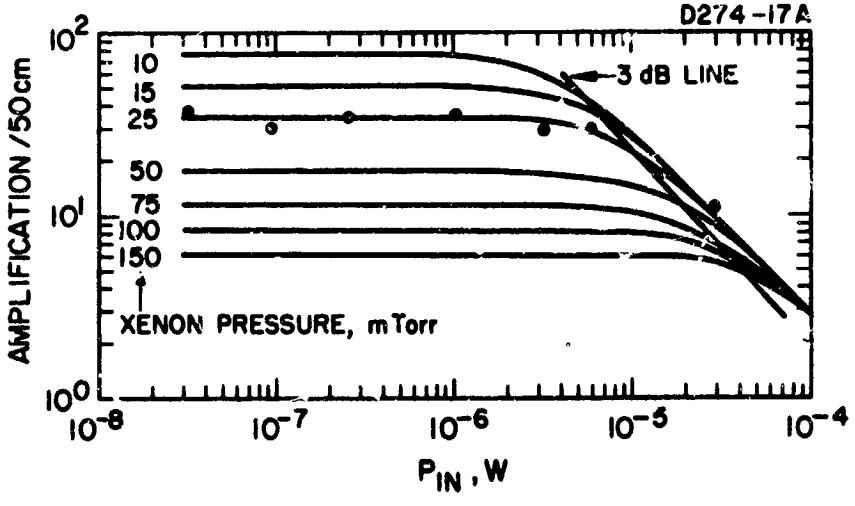

Fig. 3. Amplification at 3.5 μ in the 8 mm diameter amplifier.

selenide cell (obtained from Hughes Santa Barbara Research Center) operated at 193°K. Under these operating conditions of temperature and wavelength, the detectivity (for a 2π steradian field of view) is $D^* = 1.2 \times 10^{10}$ cm-sec$^{-1/2}$/W. A Millivac VS68B hushed amplifier was used between the detector and the lock-in amplifier. The entire detection system was calibrated by measuring the power with an Eppley thermopile located at the detector position; the laser amplifier and chopper were off. The minimum detectable signal level was of the order of 10^{-8} to 10^{-9} W.

C. Observations and Results

1. Variation of Optical Gain with Input Power and Pressure

Optical amplification at 3.508 μ was measured for input powers ranging from approximately 10^{-4} to 10^{-9} W. For even the highest gain observed, the 10^{-9} W input was small enough to permit determination of small signal gain under those operating conditions. Figures 3, 4, and 5 illustrate the variation of optical gain as a function of xenon pressure and input power for the 8, 5.1, and 2.6 mm diameter amplifiers, respectively. To avoid cluttering the diagrams unnecessarily, the experimental points are indicated for only one pressure in each amplifier. The spread in the data is representative of the variation observed at all pressures. For each combination of diameter and pressure, the discharge current was optimized for maximum amplification.

With each amplifier the maximum small gain was observed at the lowest pressure investigated (10 mTorr). For the 8, 5.1, and 2.6 mm bore amplifiers, these maximum gains were approximately ~~20~~ 38, 54, and ~~35~~ dB/m, respectively. The absence of an optimum pressure in the 10 to 150 mTorr range indicates that an earlier determination of optimum xenon pressure[5] may be in error. This can be attributed to the difficulty (resulting from rapid gas cleanup) in maintaining a uniformly low (< 15 mTorr) xenon pressure. This effect is further increased by the relatively large discharge currents necessary for maximum amplification at low pressures. In the present experiment it was necessary, when operating in the low pressure regime, to leak xenon continually into the amplifier in order to maintain a constant pressure.

It is obvious from Figs. 3, 4, and 5 that gain saturation occurs at very low input powers. In diagrams 3 and 5 a line has been drawn through the points at which the gain is reduced by 3 dB. For the 8 mm diameter tube this line corresponds to a constant output power of 0.23 mW. Similar pressure independence of gain saturation has been observed in a 5 mm bore amplifier.[5] This relation does not hold for the 2.6 mm diameter tube. Here the output power at the 3 dB points varies uniformly from 70 μW at a xenon pressure of 10 mTorr to 42 μ W at 150 mTorr.

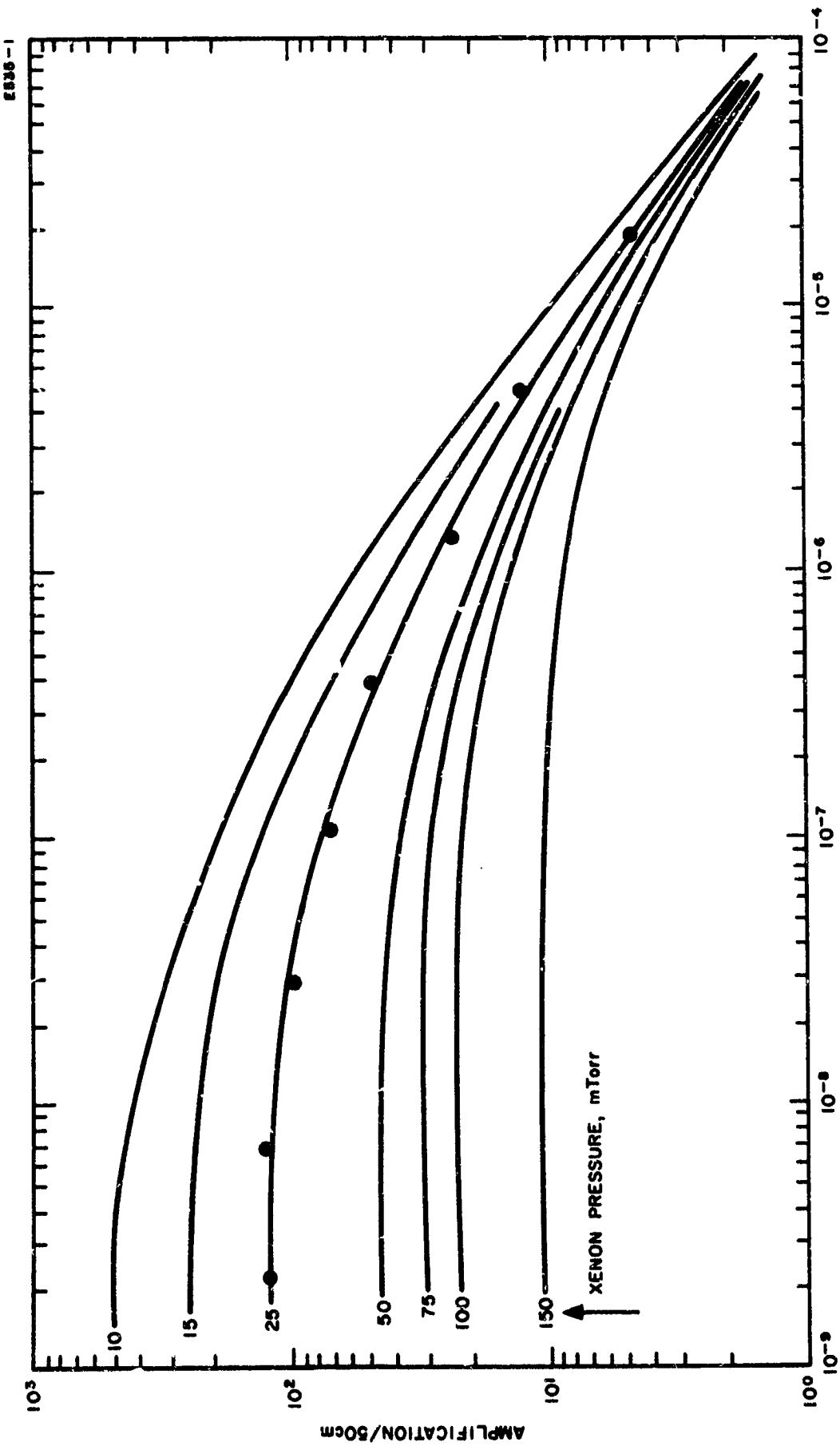

Fig. 4. Amplification at 3.5 μ in the 5.1 mm diameter amplifier.

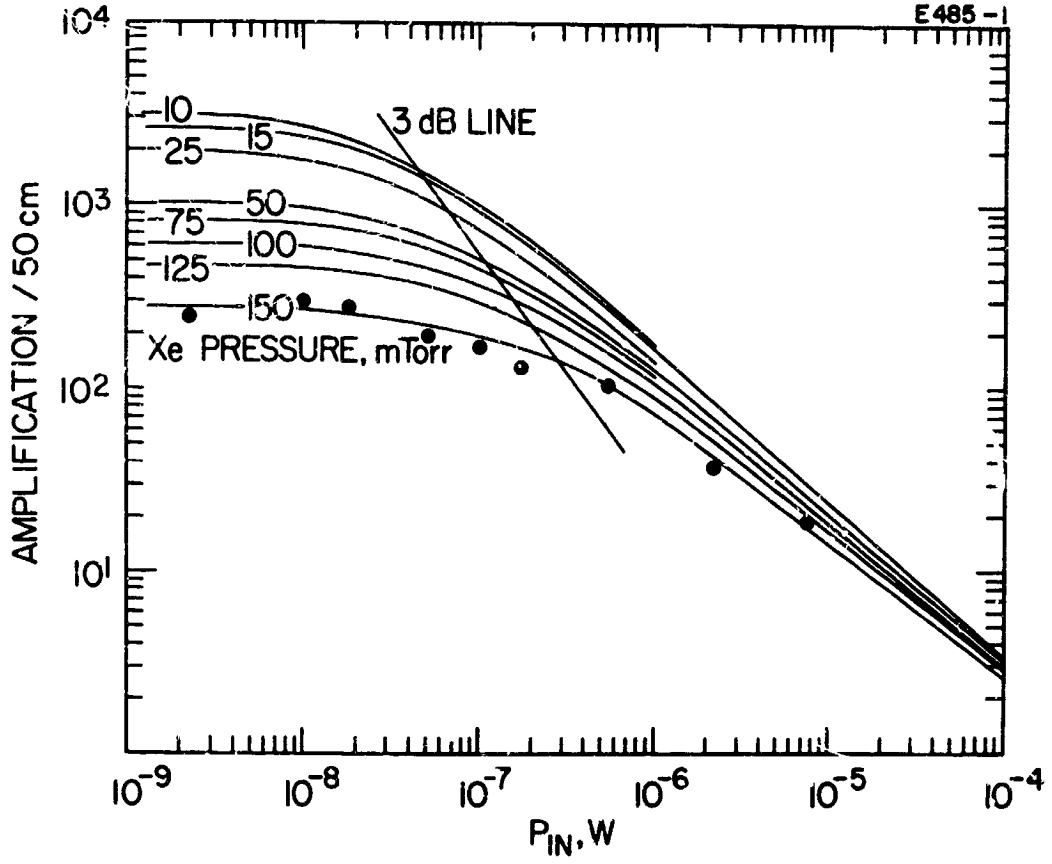

Fig. 5. Amplification at 3.5 μ in the 2.6 mm diameter amplifier.

From the behavior of the saturated portions of the amplification curves one should be able to obtain some information regarding the particular type of line broadening occurring in the amplifier. It has been shown[6,7] that for homogeneous and inhomogeneous line broadening, the gain coefficient g and the radiation intensity w (at a fixed plane in the medium) satisfy the following equations

$$\text{Homogeneous,}\quad g = \frac{g_o}{1 + \frac{w}{w_o}} \tag{1a}$$

$$\text{Inhomogenous,}\quad g = \frac{g_o}{\left(1 + \frac{w}{w_o}\right)^{1/2}} \quad . \tag{1b}$$

In both cases g_o is the unsaturated gain coefficient. In (1a) w_o is the radiation intensity at which the gain coefficient decreases to $g_o/2$ and in (1b) it is the value at which g falls to $g_o/\sqrt{2}$.

Rigrod[7] has demonstrated that for a lossless amplifier of length L and for high signal levels ($w/w_o >> 1$), eqs. (1a) and (1b) may be integrated to yield

$$\text{Homogeneous,}\quad g_oL = \left(\frac{w_2}{w_o} - \frac{w_1}{w_o}\right)\left(1 + \frac{w_o}{w_1}\right) \tag{2a}$$

$$\text{Inhomogeneous,}\quad \frac{g_oL}{2} = \left(1 + \frac{w_2}{w_o}\right)^{1/2} - \left(1 + \frac{w_1}{w_o}\right)^{1/2} \tag{2b}$$

where w_1 and w_2 are the input and output intensities, respectively. The net amplifier gain is defined as $G = w_2/w_1$. Then it follows from (2a) that

$$G = 1 + \frac{g_o}{1 + (w_1/w_o)} \cong 1 + \frac{g_oL}{w_1/w_o} \quad . \tag{3a}$$

From (3a) it is evident that in the saturated portion of the amplification curves (i.e., for high input intensities), in the case of homogeneous broadening the quantity (G - 1) exhibits the same -1 power dependence as the gain coefficient g (refer to (1a)).

With the additional requirement that the over-all amplifier gain G be small in the saturated portion of the gain curve, it can be shown that for inhomogeneous broadening

$$G \cong 1 + \frac{g_o L}{(w_1/w_o)^{1/2}} \quad . \tag{3b}$$

Thus for inhomogeneous line broadening the quantity (G - 1) also demonstrates the same - 1/2 power dependence as the gain coefficient g under highly saturated conditions.

Equations (3a) and (3b) indicate that regardless of the type of line broadening, the net amplifier gain asymptotically approaches unity with increasing input intensity. Figures 3, 4, and 5 indicate that for all the amplifiers the experimental results do approach unity gain at sufficiently large input power, as is required. In Fig. 6 the quantity (G - 1) is plotted for two of the amplifiers at high input powers. The particular xenon pressure chosen is 150 mTorr; however, it is apparent from Figs. 3, 4, and 5 that in the saturation region each amplifier behaves uniformly at all pressures in the range 150 to 10 mTorr. At high input powers the slopes of both curves in Fig. 6 are close to - 1. This is to be expected in this experiment. Since the output line width of the superradiant oscillator is very close to that of the amplifier, the gain decreases proportionately over the entire transition line and the amplifier behaves as though it were homogeneously broadened.

2. Pressure-Diameter Relation

In dc-excited xenon discharges, the dominant electron loss mechanism is that resulting from wall collisions.[8] Under these conditions, the average electron energy is determined primarily by the product pd,[9] and the total energy per unit length of the plasma electrons is proportional to pd^3. Since the atomic processes leading to high gain at 3.5 μ involve electron impact excitation only,[10, 11] one would expect that the gain of the medium might have some dependence on the pd^3 parameter.

Over the pressure range investigated (10 to 150 mTorr) the observed dependence between xenon pressure and tube diameter is of the form $pd^n = C$ where $n \cong 3.2 \pm 0.2$, and C decreases monotonically with increasing gain. This result implies that in order to approximately maintain a specified gain under optimum operating conditions, it is sufficient that amplifiers of different diameters and pressures satisfy a pd^3 scaling law.

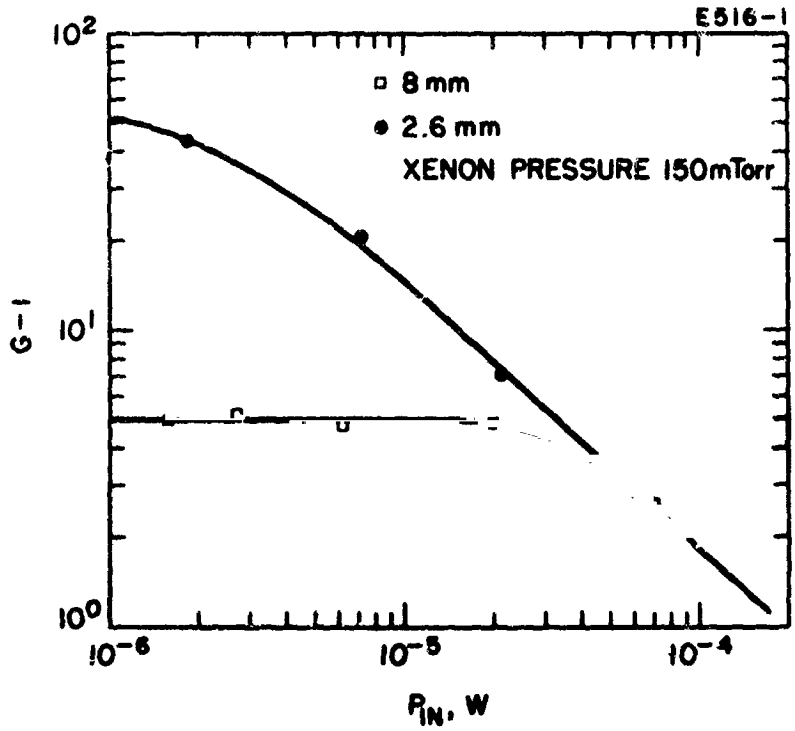

Fig. 6. Variation of (G - 1) in the highly saturated operating region. (G = net amplifier gain.)

3. Gain-Diameter Relation

Figure 7 shows the variation of small-signal optical gain expressed in decibels as a function of tube radius with gas pressure as a parameter. These curves also demonstrate the dependence of population inversion density on tube diameter and gas pressure because the gain (in decibels) is proportional to $(n_2/g_2) - (n_1/g_1)$ for small signal amplification. It is evident that for large bore tubes (radius $\gtrsim$ 3.5 mm), the gain (inversion density) is proportional to $(\text{radius})^{-1}$. This dependence has previously been observed by other investigators.[11] For smaller bore amplifiers, the gain appears to vary as $(\text{radius})^{-n}$, where $n > 1$ for xenon pressures greater than 50 mTorr and $n < 1$ for pressures less than 50 mTorr. A similar variation with $n \cong 2$ has been observed in a 1 mm diameter, 0.63 μ helium-neon laser.[12]

4. Estimate of Relative Power Output

One of the objectives of this program was to demonstrate a simple design technique for xenon oscillators based on information obtained from the gain measurements. Rigrod[7] has presented a detailed treatment of single and multimode oscillators and has performed experiments at 1.15 μ in helium-neon with a 1.75 m cavity which verify his theoretical conclusions. An interesting result of his experiments is that in a multi-transverse mode oscillator, the gain saturates independently at each frequency. At the same time there is no reason to assume that each mode saturates in a very different fashion.

On this basis it is reasonable to believe that with a complete neglect of the transverse mode distribution, it is possible to perform a simple calculation which is a good design approximation to the relative variation of output power with mirror reflectivity for an oscillator whose axial modes are not closely spaced. This calculation is outlined below.

The threshold oscillation condition for a laser with one mirror perfectly reflecting and the other of reflectivity R is

$$G_L^2 \gamma^2 T^2 R = 1 \qquad (4)$$

where

G_L = single pass gain $= e^{\int_0^L g\,dz} \cong e^{gL}$

$1 - \gamma$ = fractional diffraction loss per pass

T = transmission of windows, etc., within the cavity.

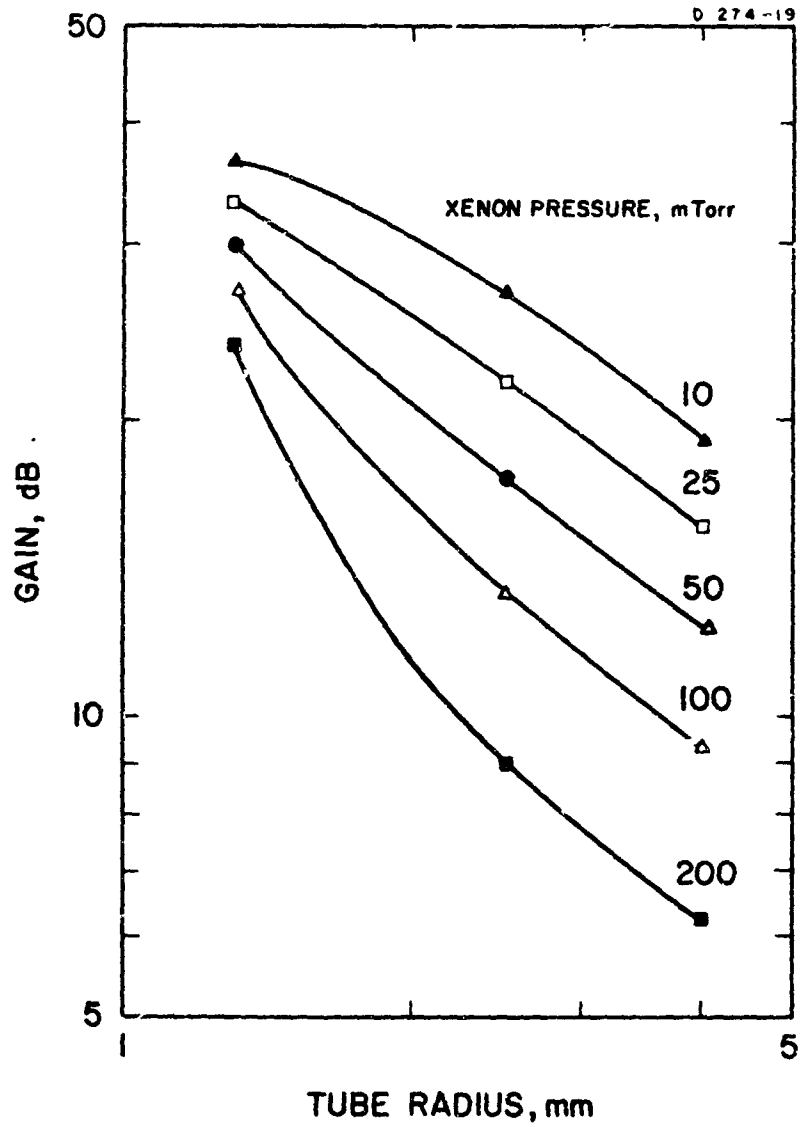

Fig. 7. Variation of small signal optical gain with tube radius.

Neglecting diffraction losses, eq. (4) may be rewritten as

$$G = \frac{1}{R^{1/2}} \tag{5}$$

where $G = G_L T$ is the quantity measured in this experiment. Assuming no absorption in the transmitting mirror, the output power is

$$P_{output} = (1 - R)P_{inside} \quad . \tag{6}$$

For a specified R, P_{inside} is obtained from a curve similar to that of Fig. 3, using (5). The output power is then calculated from (6). Figure 8 illustrates this calculation for the 8 mm diameter tube at a xenon pressure of 75 mTorr. Two experimental points are also indicated. These values were obtained by operating the amplifier as an oscillator with two different cavity configurations, an aluminized spherical mirror with a quartz flat ($R \cong 0.05$), and with a multilayer dielectric mirror ($R \cong 0.75$). In both cases the mirror spacing was 60 cm, which corresponds to an axial mode spacing of 250 Mc.

In calculating Fig. 8, the highly saturated portion of the gain curve is used. Increasing or decreasing the amplification length will shift this portion of the curve to higher or lower powers and leave it essentially undistorted. Thus, to the extent that the axial mode distribution can be neglected, the curve in Fig. 8 will shift up or down but the relative power output as a function of reflectivity will remain essentially unchanged. It is evident from Fig. 8 that for a cavity with one transmitting mirror, the optimum reflectivity is in the range 0.25 to 0.40. A multitransverse mode laser was constructed with a germanium flat as the output mirror for use in the spectroscopy measurements discussed in Section III. This mirror has a reflectivity of about 0.36. With this configuration the power output at 3.508 μ was increased significantly over that obtained with a quartz flat or a multilayer dielectric mirror.

5. Discharge Power and Oscillator Efficiency

The discharge power required by the three amplifiers is shown as a function of gas pressure in Fig. 9. In each case the necessary discharge power for maximum gain decreases as the pressure increases. Although the power required by each amplifier varies at pressures less than 40 mTorr, the discharge power for maximum gain is independent of tube diameter at higher pressures.

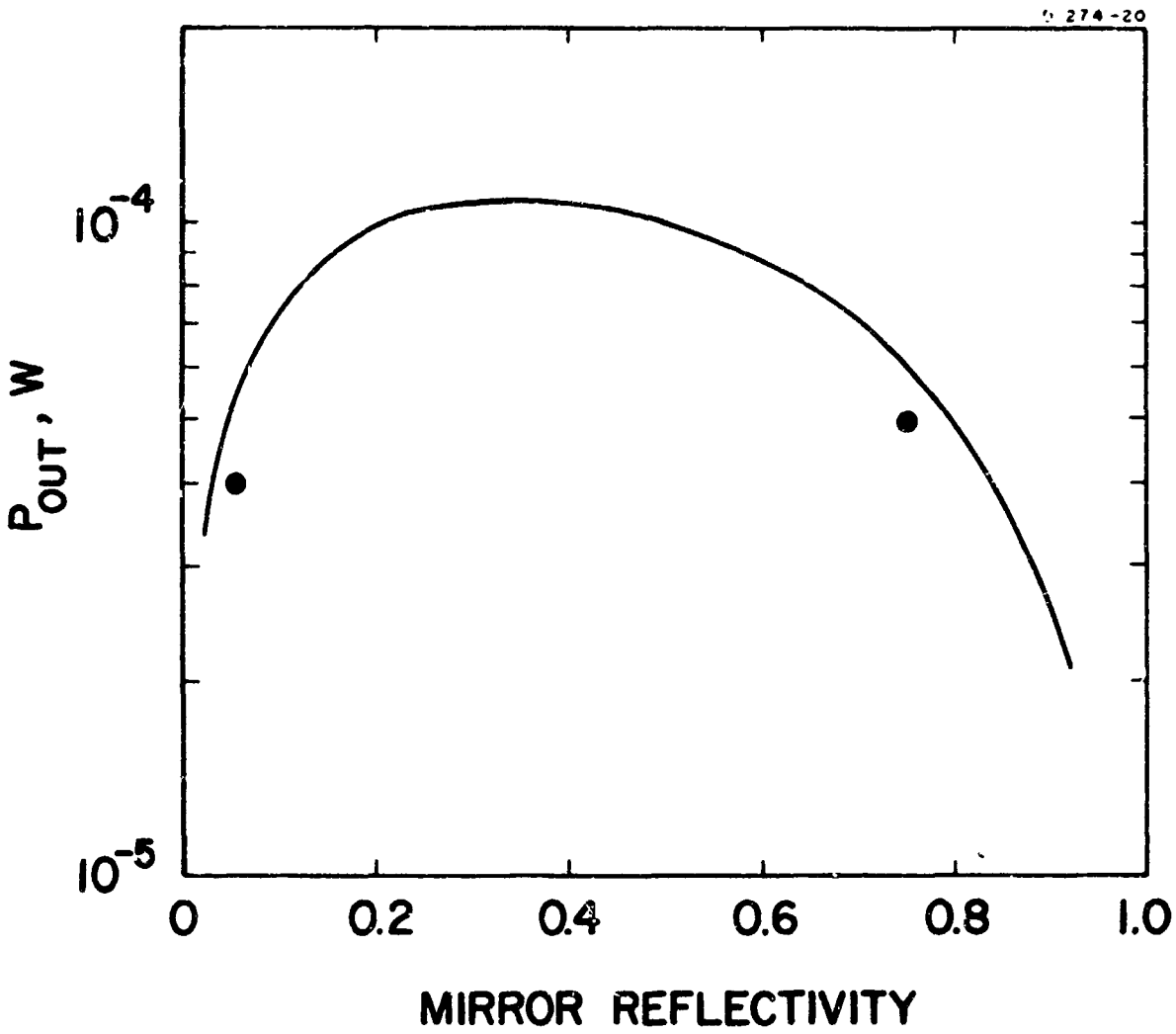

Fig. 8. Predicted output power from a cavity with one mirror perfectly reflecting and the other of reflectivity R. (Pressure = 75 mTorr; tube diameter = 8 mm; discharge length = 50 cm.)

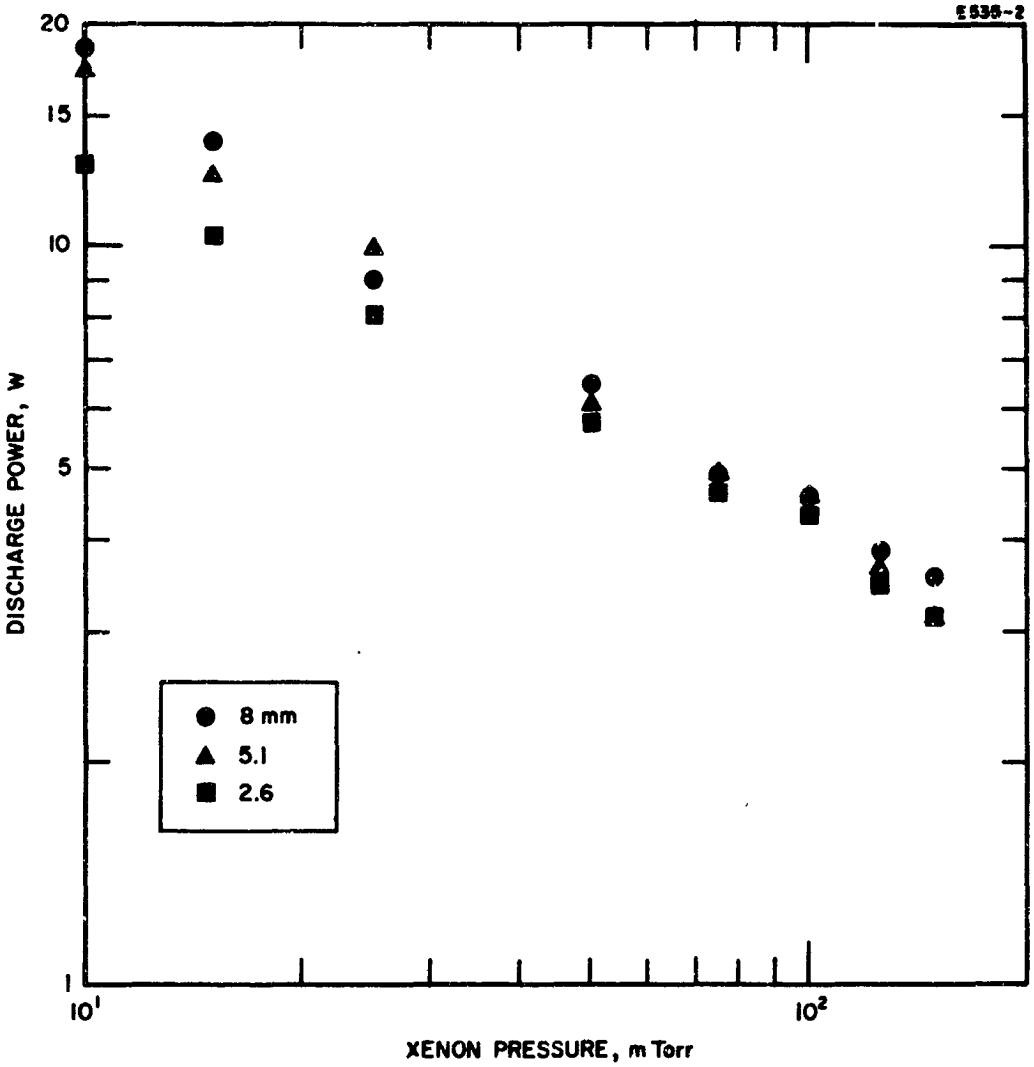

Fig. 9. Variation of discharge power with gas pressure.

It was indicated in Section II-C-4 that, as an oscillator, the laser operates in the saturated portion of its gain versus input power curve. Figures 3, 4, and 5 demonstrated that under these operating conditions all the amplifiers behave similarly, and produce approximately the same total output power in a transverse mode distribution which fills the discharge cross section. Under these conditions the efficiency is independent of tube diameter. However, with a mirror configuration which suppresses all but the lowest order transverse mode (e. g., a curved mirror and a "dot" reflector at the near-hemispherical spacing), the output power and efficiency will decrease as the tube diameter increases.

D. Conclusions

Measurements of optical gain at 3.508 μ in pure xenon dc-excited discharges were completed for a wide range of xenon pressures and tube diameters. The results of this experiment illustrate the availability of very high small signal gain. In the present experiment a small signal gain of 70 dB/m was measured in a 2.6 mm bore amplifier at a xenon pressure of 10 m Torr. No optimum gas pressure was observed in the 10 to 150 mTorr range. The small signal optical gain increased monotonically as the pressure decreased for all amplifier diameters.

The results of this investigation indicate an approximate $pd^3 = C$ relation, where p is the gas pressure, d is the tube diameter, and C is a constant which decreases uniformly as the small signal gain increases. For large diameter tubes (i. d. $\geq$ 7 mm) the small signal gain varies as the radius. However, in small bore tubes (i. d. $\leq$ 3 mm), a complicated pressure dependent variation was observed.

Regardless of the tube diameter, the small signal optical gain saturates at low signal levels. As a result, the conventional xenon laser cannot produce high output powers. When operating as multi-transverse mode oscillators, the power output and efficiency of the lasers are approximately independent of the tube diameter. However, when oscillating in the lowest order transverse mode, both power output and efficiency decrease as the bore diameter increases.

III. SPECTROSCOPY OF THE DC-EXCITED XENON LASER

A. Introduction

The majority of the laser lines occurring in the dc-excited xenon discharge result from 5d-6p transitions. The pertinent energy levels are shown in Fig. 10. In addition, there are several 7p-7s, 5d'-7p, 5d'-4f, and unassigned transitions. However, the 5d-6p group is of most interest here since it includes the 3.5080 μ line.

The intensity of several spontaneously emitted lines was monitored as a function of discharge current and gas pressure. These included lines which directly involved either the upper ($5d[7/2]^0_3$) or lower ($6p[5/2]_2$) energy level of the 3.5080 μ transition as well as spontaneous emission at several laser frequencies. The current and pressure dependence of several laser lines was also investigated. Of the 29 known laser transitions in xenon, 15 were observed. These were not all seen simultaneously since their occurrence is dependent on the resonator mirrors, mirror spacing, discharge length, gas pressure, and discharge current. In addition, several lines were observed which have not previously been reported in the literature.

B. Apparatus

The experimental apparatus used in the spectroscopic measurements is shown in Fig. 11. As in the gain measurements discussed in Section II, a phase-locked detection system is used which permits the extraction of low level signals from the background noise. Two lasers were used in these experiments, one 50 cm long with an 8 mm i.d., and the other 1 m long with a 4 mm i.d. Both tubes were provided with sodium chloride Brewster angle windows to obtain better than 80% transmission at wavelengths up to 15 μ. To decrease the effect of cataphoresis in noble gas mixtures, the lasers were constructed with gas return paths. M_1 was an aluminized spherical mirror and the output mirror M_2 was a germanium flat (with approximately 36% reflectance and 50% transmittance for $1.8\ \mu < \lambda < 12\ \mu$) or an aluminized flat with a 1 mm diameter coupling hole.

M_3 and M_4 were aluminized front surface mirrors which focused the output radiation from the laser onto the entrance slit of a Model 98 Perkin-Elmer Monochromator. Dense flint, lithium fluoride, and sodium chloride prisms provided adequate dispersion for wavelengths shorter than 15 μ. The detector was a vacuum thermocouple with a cesium iodide window. A 10 cps chopper provided a reference signal for the lock-in amplifier (Princeton Applied Research Model JB-5). When the laser radiation was scanned, the output from the lock-in amplifier was applied to a chart recorder driven synchronously with the spectrometer.

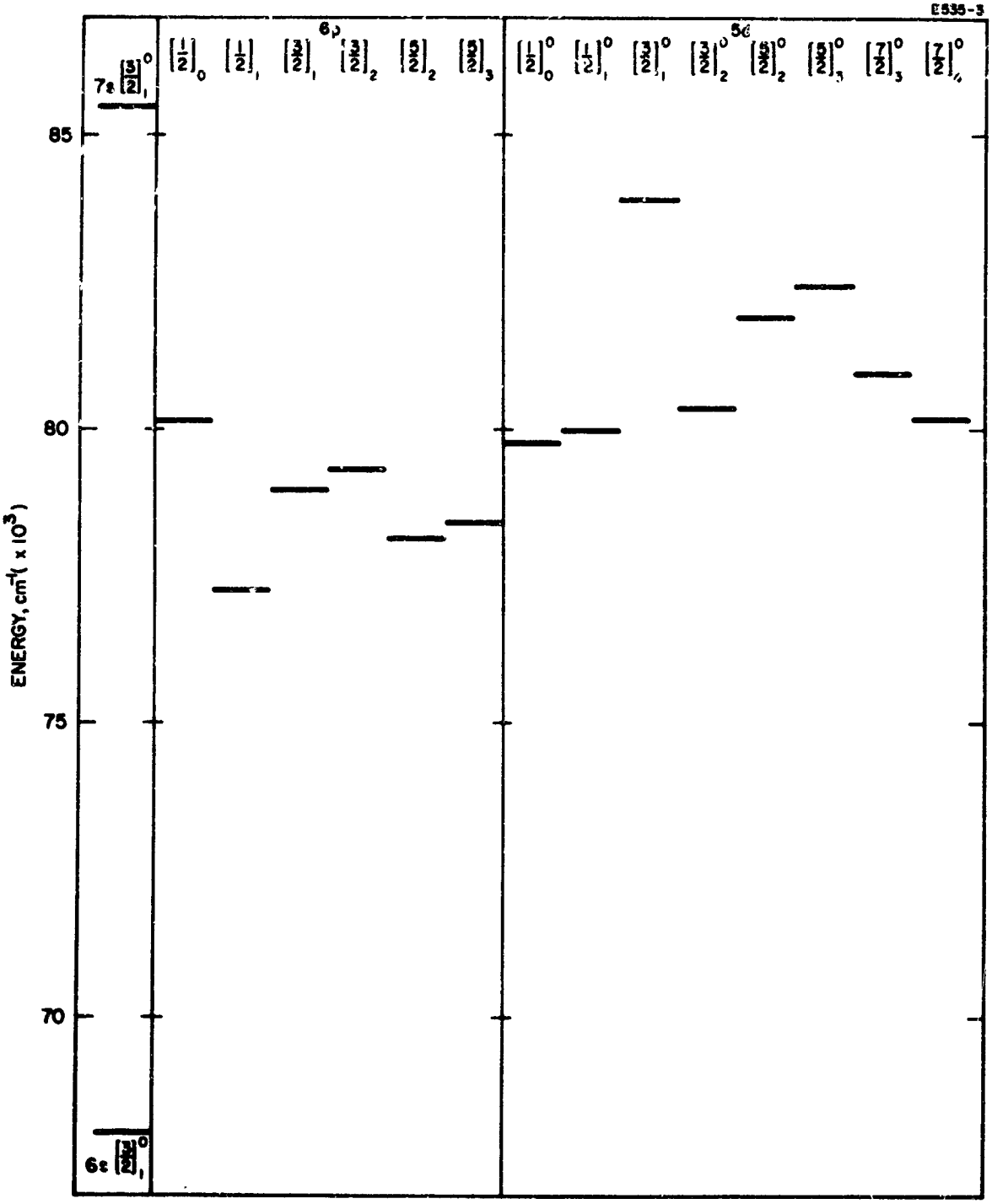

Fig. 10. Energy levels pertinent to the spectroscopic investigation of laser action in xenon.

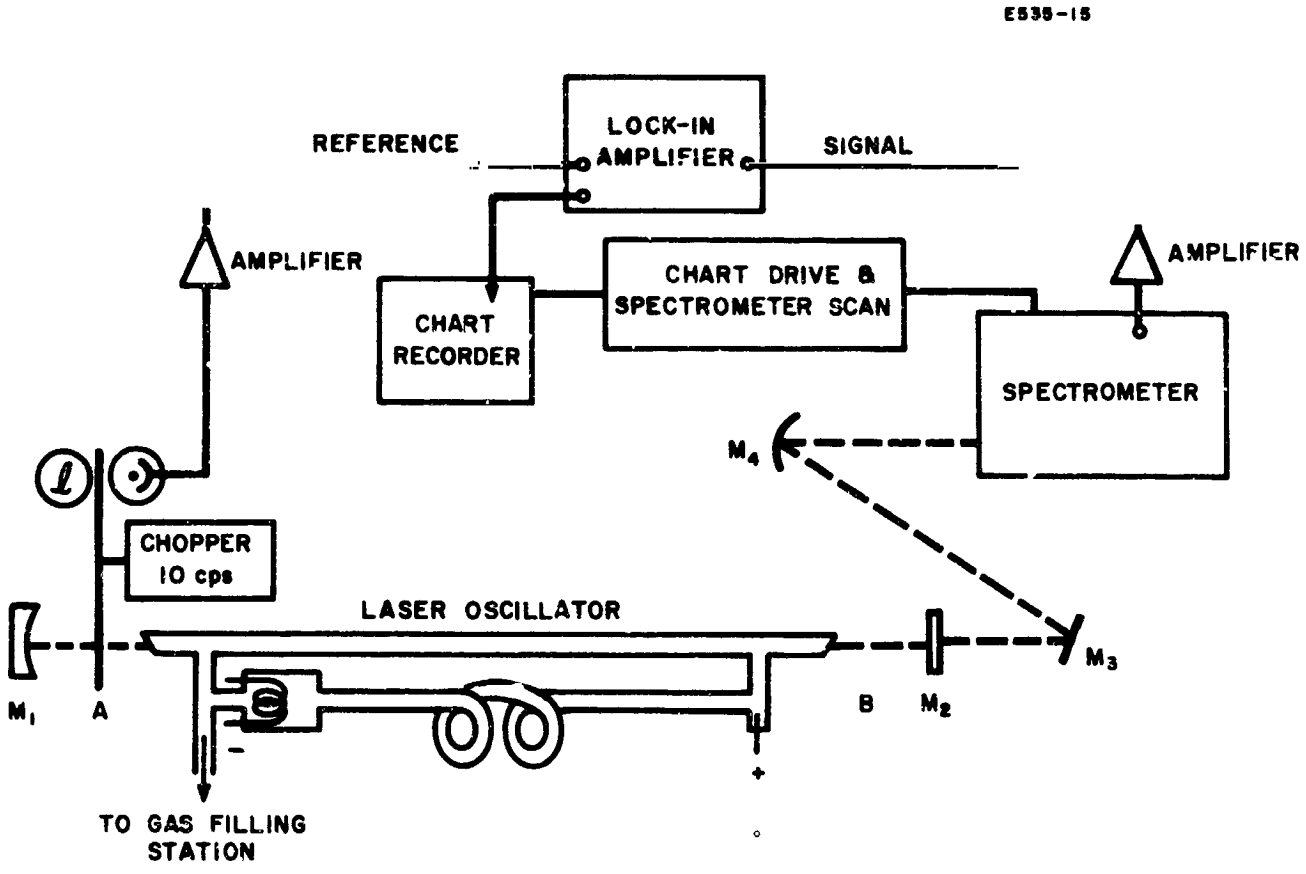

Fig. 11. Experimental system to observe stimulated emission in xenon.

The apparatus shown in Fig. 11 was used to observe stimulated emission. For spontaneous emission measurements, the output mirror M_2 was removed, and the chopper position changed from A to B.

C. Spontaneous Emission

The initial investigations of spontaneous emission were attempted with the discharge tube shown in Fig. 12. However, the infrared spontaneous emission was so weak that no observations could be made.

To provide sufficient intensity, spontaneous emission was monitored with the apparatus illustrated in Fig. 11 and described in Section III-B. A typical wavelength scan obtained using the lithium fluoride prism is shown in Fig. 13. What was actually observed, however, was not simply spontaneous emission but greatly amplified spontaneous emission. This is illustrated in Figs. 14(a) and 14(b) where it is evident that for the high gain 3.5080 μ transition, both the laser and highly amplified spontaneous emission have approximately the same current dependence. The extremely high gain on many of the 5d-6p transitions is a problem in that it tends to obscure the true current and pressure dependence of spontaneous emission from the upper laser levels. The result of this "superradiance" effect is to deplete the 5d levels selectively through the very high gain transitions rather than through the usual branching ratios. Since the excitation mechanism of the upper levels is essentially independent of the presence or absence of laser action, the total number of 5d-6p transitions remains approximately constant. This leads to a set of current- and pressure-dependent branching ratios which do not represent the natural spontaneous emission processes.

The current dependence for the 3.5080 μ laser line and several spontaneously emitted lines is shown in Figs. 14(a) and 14(b) for xenon pressures of 25 and 50 mTorr, respectively. The 3.5080 μ laser and spontaneous radiation curves have been normalized to 100. The spontaneous wavelengths and their associated transitions are listed below.

Wavelength, μ	Upper Level	Lower Level
3.8950	$5d[7/2]^{o}_{3}$	$6p[5/2]_3$
3.5080	$5d[7/2]^{o}_{3}$	$6p[5/2]_2$
2.6276	$5d[5/2]^{o}_{2}$	$6p[5/2]_2$
1.3656	$7s[3/2]^{o}_{1}$	$6p[5/2]_2$
0.9923	$6p[5/2]_2$	$6s[3/2]^{o}_{1}$ (metastable)

M 3889

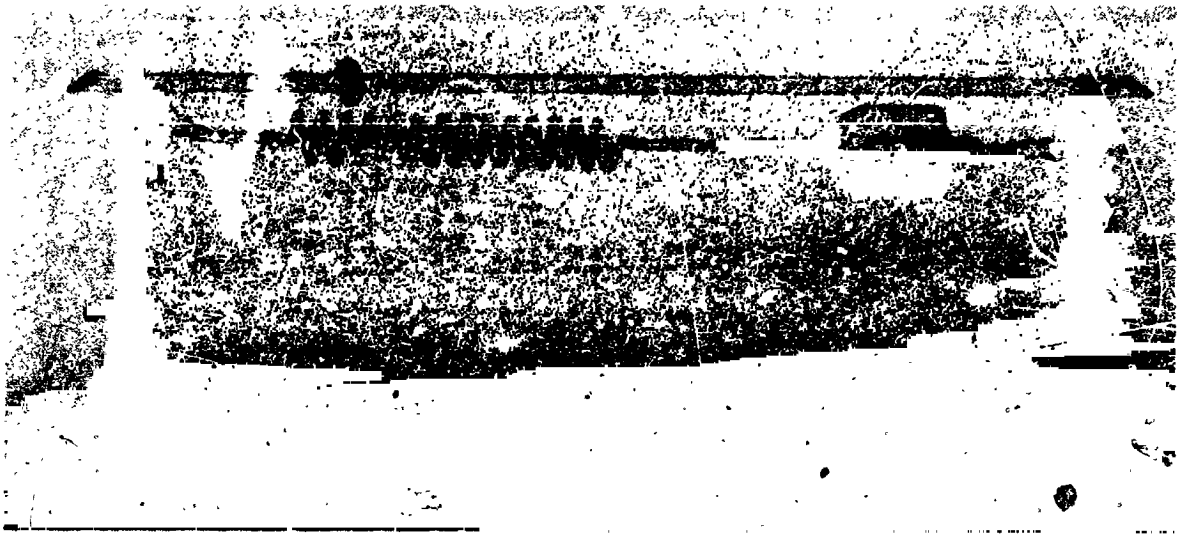

Fig. 12. Discharge tube with side windows to allow observation of spontaneous emission.

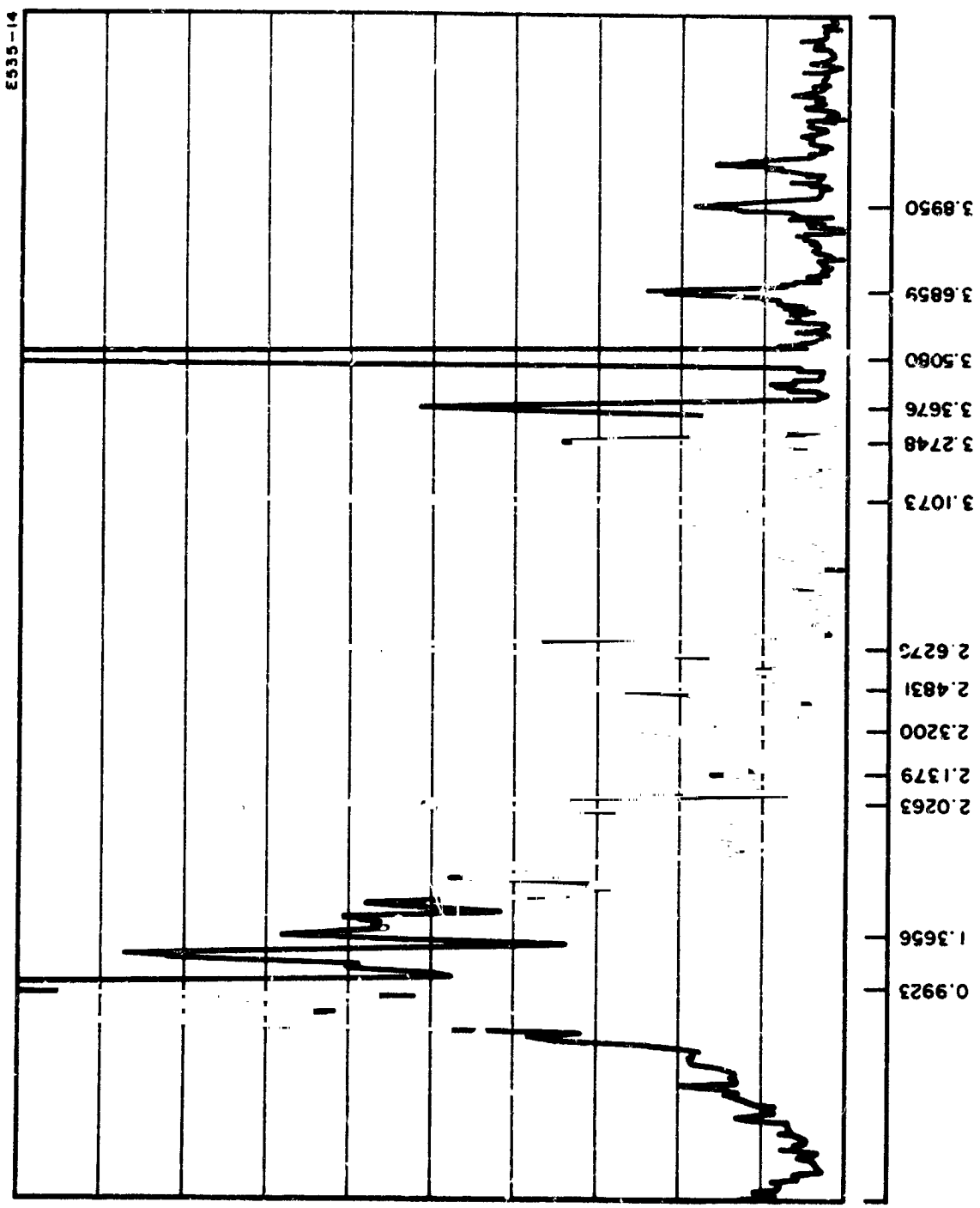

Fig. 13. Wavelength scan of spontaneous emission from a xenon discharge. $\lambda < 4\,\mu$.

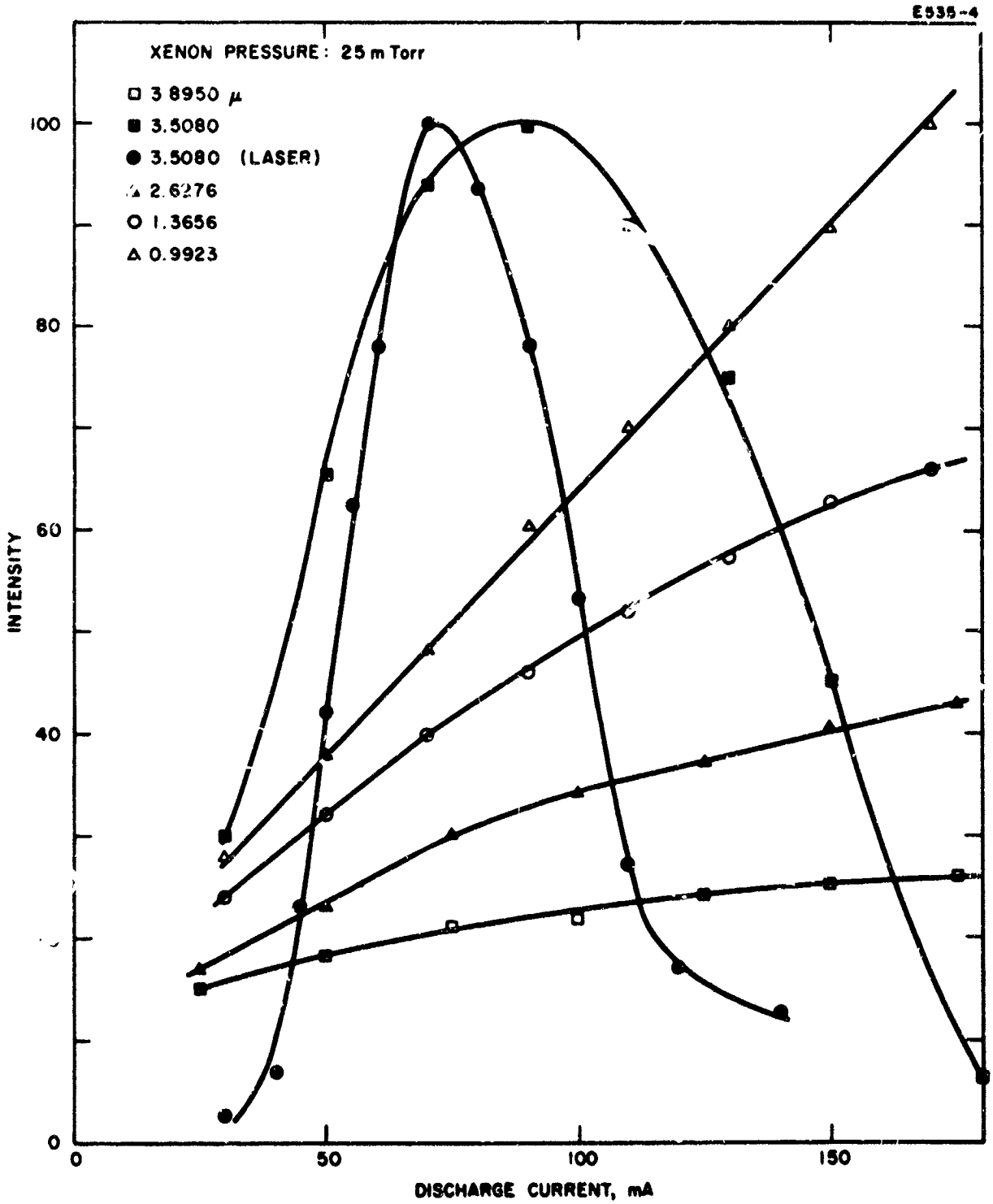

Fig. 14(a). Current variation of spontaneously emitted lines involving energy levels of the 3.5080 μ transition. Pressure 25 mTorr.

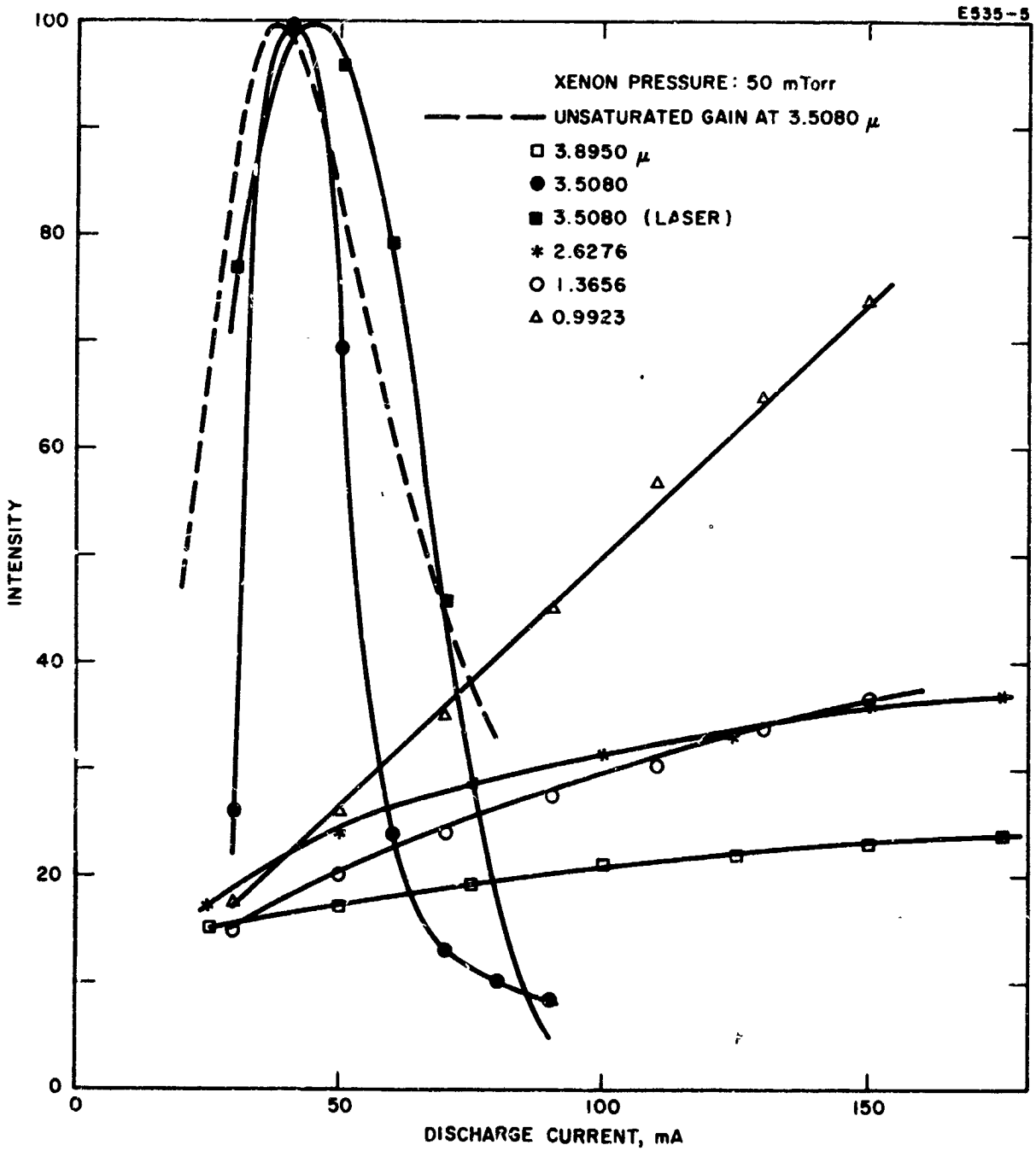

Fig. 14(b). Current variation of spontaneously emitted lines involving energy levels of the 3.5080 μ transition. Pressure 50 mTorr.

The spontaneously emitted 3.5080 μ radiation demonstrates the same general features as the laser radiation — a sharply defined optimum current for maximum intensity and a rapid decrease in intensity with increasing or decreasing current. However, the optimum current has a higher value for the laser radiation than for the spontaneous radiation. In addition, as the current is varied about its optimum value, the intensity decreases more slowly for the laser radiation than for the spontaneous radiation. Both of these effects decrease as the xenon pressure increases. Figure 14(b), showing the current dependence of the unsaturated gain (normalized to 100), indicates that the optimum current increases as the degree of saturation of the medium at 3.5080 μ increases. The unsaturated gain curve has the lowest optimum current; the superradiant case, where only part of the discharge length is saturated, has the next highest optimum current; and the laser, which is completely saturated, requires the largest optimum current.

The 0.9923 μ line joining the lower laser level to a metastable level is a strong, spontaneously emitted line whose intensity increases rapidly with current in a linear manner. Lines which terminate on the lower laser level (e.g., 1.3656 and 2.6276 μ) demonstrate a less rapid increase in intensity with current, and, at both pressures investigated, the rate of increase of these line intensities decreases markedly at approximately the optimum current for maximum 3.5080 μ intensity. The behavior of these lines may be interpreted in terms of the electron temperature of the discharge. At low currents, the number of metastables is small and the electron temperature must be high to balance the loss of charges to the wall. As the current increases, the metastable populations grow. Since the metastable atoms are more easily ionized than the ground state atoms, the electron temperature can decrease and still sustain the same losses to the walls of the discharge tube. As the electron temperature falls, the electron distribution shifts so that the number of electrons available to excite the high energy levels is decreased. Eventually the metastable population saturates and the electron temperature becomes independent of electron density.[13]

At low currents the excitation of all levels is proportional to the electron density and hence the current. Levels such as the 6p (which are connected to the ground state via forbidden transitions) are excited by single electron collisions to allowed states from the ground state followed by multiple cascading and are thus also linearly proportional to the current. As the current increases and the electron temperature drops, the rate of excitation of the higher energy levels becomes less. This is evidenced by a decrease in rate at which the intensity of the 2.6276 and 1.3656 μ lines increases with current. On the other hand, the 6p levels can now be filled by single electron impact excitation from the filled metastable levels. As a result, the increase with current of the intensity of lines such as the 0.9923 μ line (which originate from the 6p levels) does not decrease. This extra source of excitation of the 6p

levels permits their population to overtake that in the 5d levels and upset the population inversion necessary for high gain. Consequently, the intensity of the 3.5080 μ radiation begins to decrease rapidly.

The current dependence of several other spontaneously emitted 5d-6p transitions is shown in Figs. 15(a) and 15(b). The wavelengths and their corresponding energy levels are tabulated below.

Wavelength, μ	Upper Level	Lower Level
2.0268	$5d[3/2]^o_1$	$6p[3/2]_1$
2.3200	$5d[5/2]^o_3$	$6p[5/2]_2$
2.4831	$5d[5/2]^o_3$	$6p[5/2]_3$
2.6276	$5d[5/2]^o_2$	$6p[5/2]_2$
3.1078	$5d[5/2]^o_3$	$6p[3/2]_2$
3.2748	$5d[3/2]^o_2$	$6p[1/2]_1$
3.3676	$5d[5/2]_2$	$6p[3/2]_1$
3.6859	$5d[5/2]^o_2$	$6p[3/2]_2$
3.8950	$5d[7/2]^o_3$	$6p[5/2]_3$

Laser action has been observed at all of these wavelengths except 2.4831 μ.[15] However, none of the lines has sufficiently high enough gain for its spontaneous emission to demonstrate the current dependence shown by the 3.5080 μ transition.

D. Stimulated Emission

A listing of all reported [1, 11, 14-17] laser transitions is given in Table I. The table includes calculated relative transition probabilities[18] and lifetimes estimated using the Bates-Damgaard approximation.[19] The 5d-6p laser transitions which are of primary interest are retabulated in Table II. It can be seen from this listing that, of the 20 reported lines,

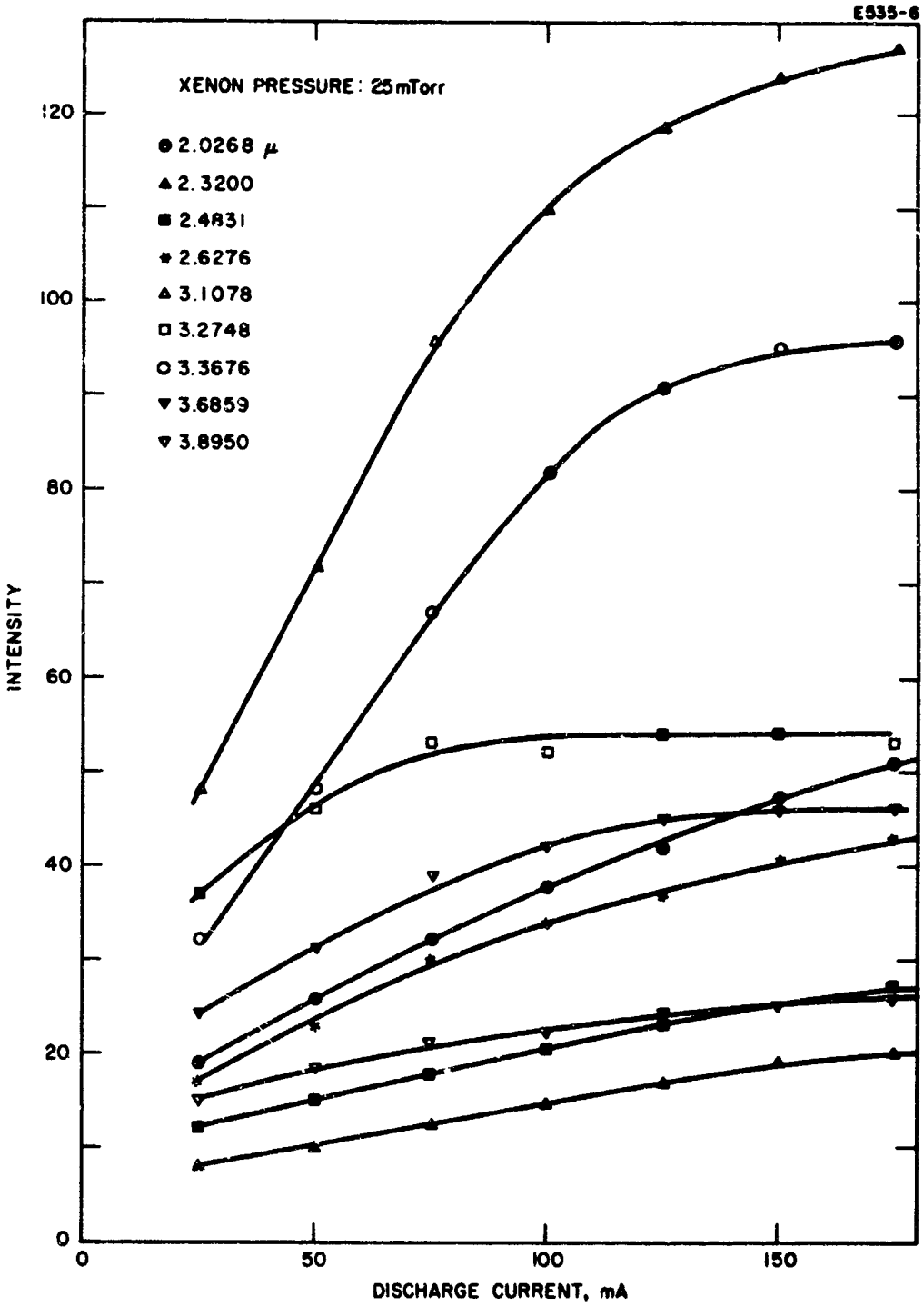

Fig. 15(a). Current variation of spontaneous 5d-6p transitions. Pressure 25 mTorr.

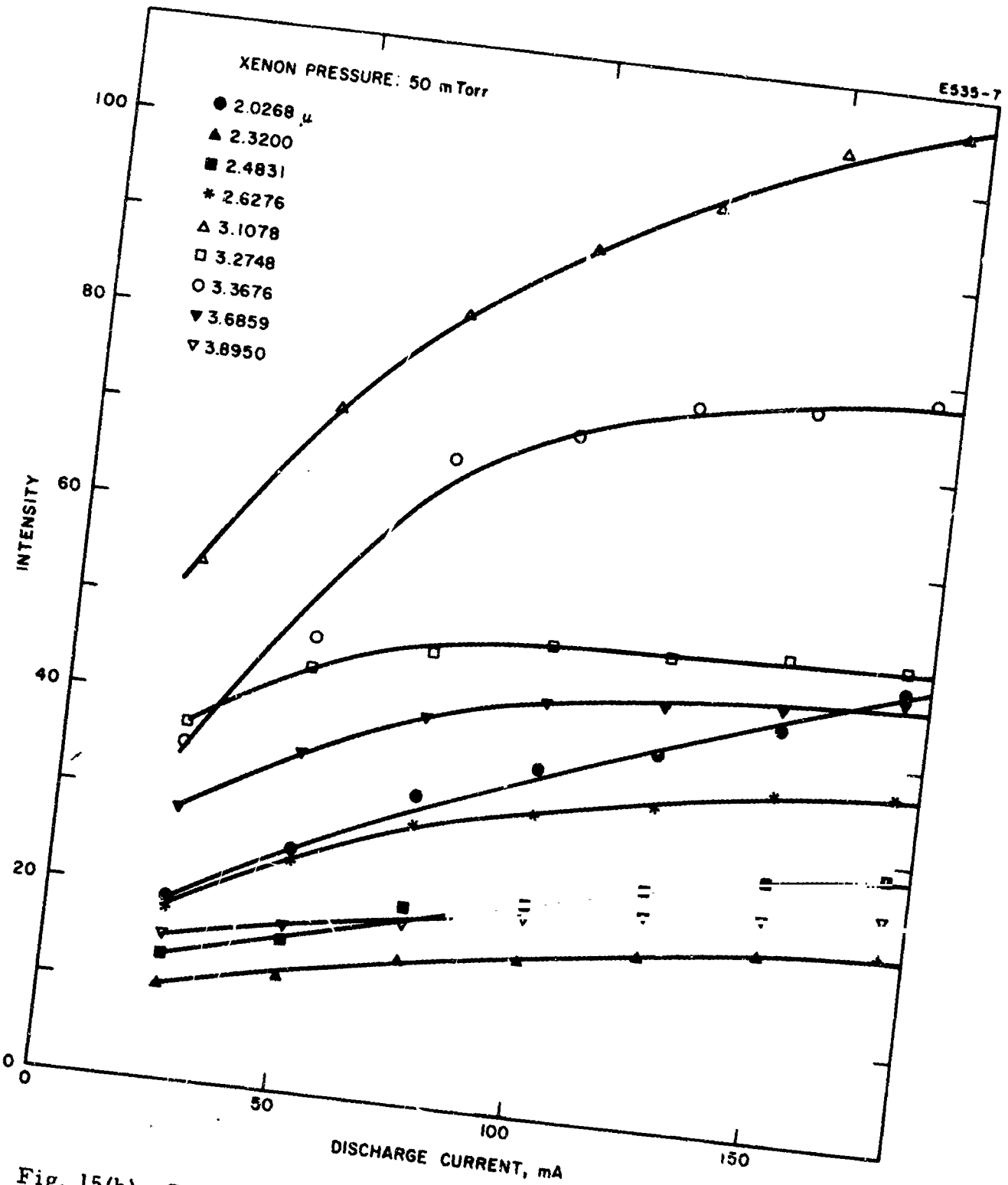

Fig. 15(b). Current variation of spontaneous 5d-6p transitions. Pressure 50 mTorr.

TABLE I

Observed Laser Transitions in Xe I

Upper Level	Lifetime, x 10-8 sec	Lower Level	Lifetime, x 10-8 sec	λ_{vac}, μ	Relative Transition Probabilities
$7p[5/2]_2$	15.5	$7s[3/2]^o_1$	5.6	3.4345	
$7p[1/2]_1$	16.1	$7s[3/2]^o_2$	5.9	3 6518	
$5d[3/2]^o_1$	24	$6p[3/2]_1$	3.4	2 0268	4/45
$5d[5/2]^o_3$	72	$6p[5/2]_2$	4.4	2.3200	1/150
$5d[5/2]^o_2$	91	$6p[5/2]_2$	4.4	2.6276	7/75
$5d[3/2]^o_1$	24	$6p[1/2]_o$	2.7	2.6518	1/18
$5d[5/2]^o_3$	72	$6p[3/2]_2$	2.7	3.1078	49/150
$5d[3/2]^o_2$	238	$6p[1/2]_1$	4.6	3.2748	5/36
$5d[5/2]^o_2$	91	$6p[3/2]_1$	3.4	3.3676	21/100
$5d[7/2]^o_3$	135	$6p[5/2]_2$	4.4	3.5080	4/9
$5d[1/2]^o_1$	275	$6p[1/2]_1$	4.6	3.6798	1/9
$5d[5/2]^o_2$	91	$6p[3/2]_2$	2.7	3.6859	7/300
$5d[7/2]^o_3$	135	$6p[5/2]_3$	3.2	3.8950	1/45
$5d[1/2]^o_o$	236	$6p[1/2]_1$	4.6	3.9966	1/18
$5d[3/2]^o_2$	238	$6p[5/2]_2$	4.4	4.5393	1/900
$5d[1/2]^o_1$	275	$6p[5/2]_2$	4.4	5.3566	
$5d[7/2]^o_4$	537	$6p[5/2]_3$	3.2	5.5754	6/10
$5d[3/2]^o_2$	238	$6p[3/2]_1$	3.4	7.3167	4/225
$5d[3/2]^o_2$	238	$6p[3/2]_2$	2.7	9.0065	4/25
$5d[1/2]^o_1$	275	$6p[3/2]_1$	3.4	9.7029	1/180
$5d[1/2]^o_o$	236	$6p[3/2]_1$	3.4	12.266	1/90
$5d[1/2]^o_1$	275	$6p[3/2]_2$	2.7	12.917	1/36
$5d'[3/2]^o_1$		$6p'[1/2]_o$		2.6608	1/9
$5d'[5/2]^o_3$		$6p'[3/2]_2$		3.8697	7/15
$5d'[3/2]^o_2$		$6p'[1/2]_1$		4.6109	5/18
$5d'[3/2]^o_2$		$7p[3/2]_2$	11.6	3.6219	
$5d'[5/2]^o_2$		$7p[3/2]_1$	13.1	4.1527	
$5d'[3/2]^o_2$		$4f[5/2]_3$		18.506	
$5d'[5/2]^o_3$		$4f[9/2]_4$		11.29	

TABLE II

Classification of the 5d-6p Laser Transitions

$p_{3/2}$ Parent Ion

Upper Level

Lower Level	$5d[1/2]^o_0$	$5d[1/2]^o_1$	$5d[3/2]^o_1$	$5d[3/2]^o_2$	$5d[5/2]^o_2$	$5d[5/3]^o_3$	$5d[7/2]^o_3$	$5d[7/2]^o_4$
$6p[1/2]_0$		(50)	2.6518 (50)					
$6p[1/2]_1$	3.9966 (50)	3.6798 (100)	(25)	3.[illegible]				
$6p[3/2]_1$	12.266 (10)	9.7029 (5)	2.0268 (80)	7.3167 (15)	3.3676 (189)			
$6p[3/2]_2$		12.917 (25)	(16)	9.0065 (144)	3.6859 (21)	3.1078 (294)		
$6p[5/2]_2$		5.3566 (10)	(9)	4.5393 (1)	2.6276 (84)	2.3200 (6)	3.5080 (400)	
$6p[5/2]_3$				(14)	(6)	(120)	3.8950 (20)	5.5754 (540)

$\Delta J = \Delta K = \Delta \ell = 1$ $\quad$ $\Delta J = \Delta K = 0$ $\quad$ $\Delta J = \Delta K = \Delta \ell = 1$

only one violates the selection rules for ℓ-J_c coupling. The bracketed numbers are the relative line strengths in 1/900 calculated by Faust and McFarlane.[20]

In the course of making the measurements reported here, most of the 5d-6p laser transitions were observed. In general, the unobserved transitions coincided with those having the smallest calculated line strengths. The 12.266 and 12.917 μ lines were difficult to observe since these transitions have a narrow Doppler width (~25 Mc) and the smallest possible axial mode spacing was ~100 Mc. Careful tuning of the resonator mirrors permitted these lines to oscillate; however, temperature variations and mirror vibrations prevented uniform measurements. It was observed that although oscillation at 7.3167 μ was extremely sensitive to mirror adjustment, substantial power output was obtained when laser action began. This indicates that this transition may have an anomalously narrow Doppler line width. Another interesting result of these experiments was a measured output power at 9.0065 μ from the 50 cm long, 8 mm i.d. laser of approximately 12 mW. This is substantially more than that obtained by other investigators using larger and more complicated laser structures.

None of the 7p-7s, 5d'-7p, and 5d'-4f transitions was observed. Of the three reported 5d'-6p' lines, only at 4.6109 μ was oscillation noted. In addition to the previously reported lines, oscillation was also observed at 6.4 and 8.2 μ. Unfortunately, the nature of the apparatus was such that it was difficult to measure wavelengths to an accuracy greater than a tenth of a micron. With this resolution, definite term assignments are difficult since there are 48 transitions which satisfy the strict selection rule $\Delta J = 0 \pm 1$ and fall in the wavelength region 6.4 ± 0.1 μ, and 25 transitions in the region 8.2 ± 0.1 μ.[21] On the weak basis that the transitions with lowest energy upper levels would be the most probable, tentative term assignments might be as follows.

Levels		Wavenumber, cm^{-1}	Calculated Wavelength, μ	Measured Wavelength, μ
Upper	Lower			
$8p[3/2]_2$	$8s[3/2]^o_2$	1566.4	6.384	6.4
$8p[1/2]_1$	$8s[3/2]^o_1$	1220.9	8.191	8.2

A typical wavelength scan of stimulated emission obtained using the sodium chloride prism is shown in Fig. 16. Note that the 7.3167 μ line appears in the 1.0 but not in the 0.1 signal level scan, even though

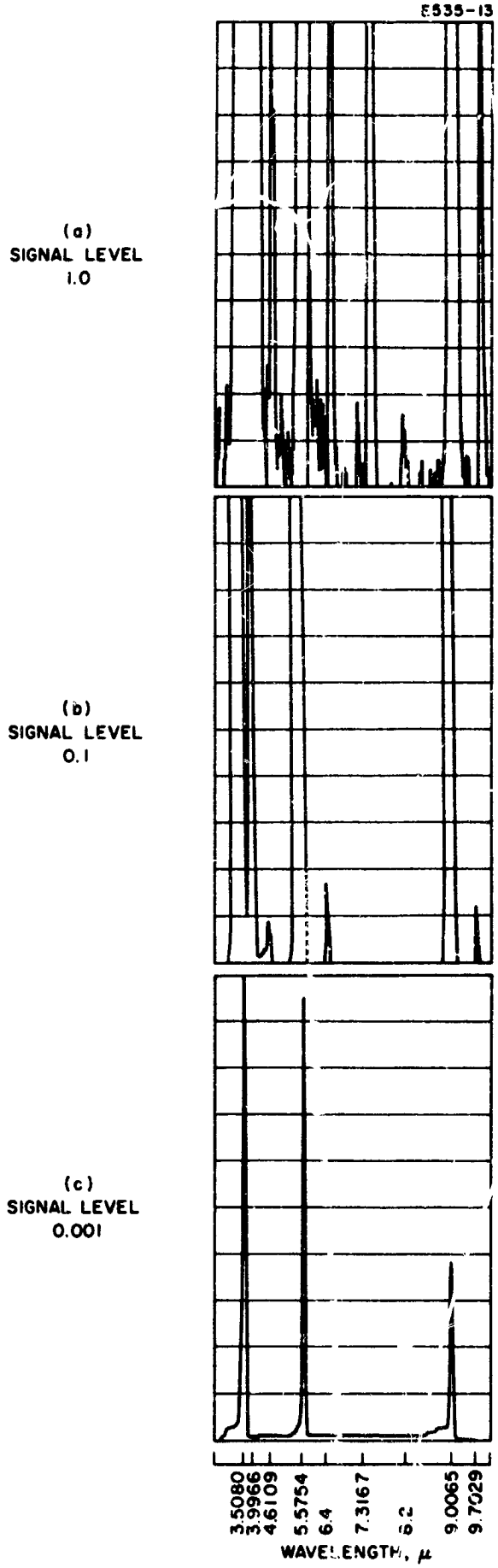

Fig. 16.
Wavelength scan of stimulated emission from a dc xenon discharge. $\lambda < 9.7\mu$.

it is sufficiently intense to appear in the latter. This illustrates the sensitivity of this transition to mirror adjustment, as discussed previously. When observing laser action in the 3 to 4 μ wavelength range, the lithium fluoride prism was used in order to obtain more dispersion.

Figures 17(a) and 17(b) illustrate the current dependence of several simultaneously oscillating wavelengths at xenon pressures of 25 and 50 mTorr, respectively. An obvious characteristic of both diagrams is that the lines tend to separate into distinct groups having different optimum currents: 3.6798, 5.5754, and 6.4 μ have the lowest optimum current; 3.5080, 3.9966, and 4.6109 μ have the next highest optimum current; and 7.3167, 9.0065, and 9.7029 μ require the highest discharge current. Of the nine lines observed, only the 4.6109 and 6.4 μ lines are not 5d-6p transition. It was shown in Section III-C that as the discharge current is increased, the population of the 6p levels begins to overtake that of the 5d levels and the gain of the 5d-6p transitions decreases. The 7.3167, 9.0065, and 9.7029 μ groups have the largest optimum current and terminate on the highest lying (except for the $6p[1/2]_0$) energy level pair, $6p[3/2]_{1,2}$ (refer to Fig. 10). This may appear to indicate that as the electron density increases, low energy 6p levels and then higher energy 6p levels, begin to be filled. Such a process would require that the 3.6798 and 3.9966 μ transitions have the lowest optimum current and that the 3.5080 and 5.5754 μ lines have the next highest optimum current. Because this grouping is not followed, however, such a simple description of the filling of the 6p levels is inadequate.

E. Xenon-Krypton Laser

A xenon-krypton laser[22] was operated to investigate the possibility of enhanced output due to excitation of the 5d xenon levels via collisions of the second kind with the two 5s krypton metastable levels. The pertinent energy levels are illustrated in Fig. 18. The indicated spins are those assigned by Moore.[21] In order to satisfy the Wigner spin rule, the following excitations would be most probable:

$$Kr(5s[3/2]_1^o) + Xe(^1S_o) \rightarrow Kr(^1S_o) + Xe(5d[7/2]_3^o), \quad \Delta E = 13.4 \text{ cm}^{-1}$$

$$Kr(5s[3/2]_2^o) + Xe(^1S_o) \rightarrow Kr(^1S_o) + Xe(5d[1/2]_1^o), \quad \Delta E = 14.6 \text{ cm}^{-1} .$$

If such collisions are efficient excitation processes, there would be an increase in the intensity of the 3.6789, 9.7029 and 12.917 μ lines which originate from the $5d[1/2]_1^o$ level and in the intensity of the 3.5080 and 3.8950 μ lines which originate from the $5d[7/2]_3^o$ level. No increase in power output was observed in the present experiment.

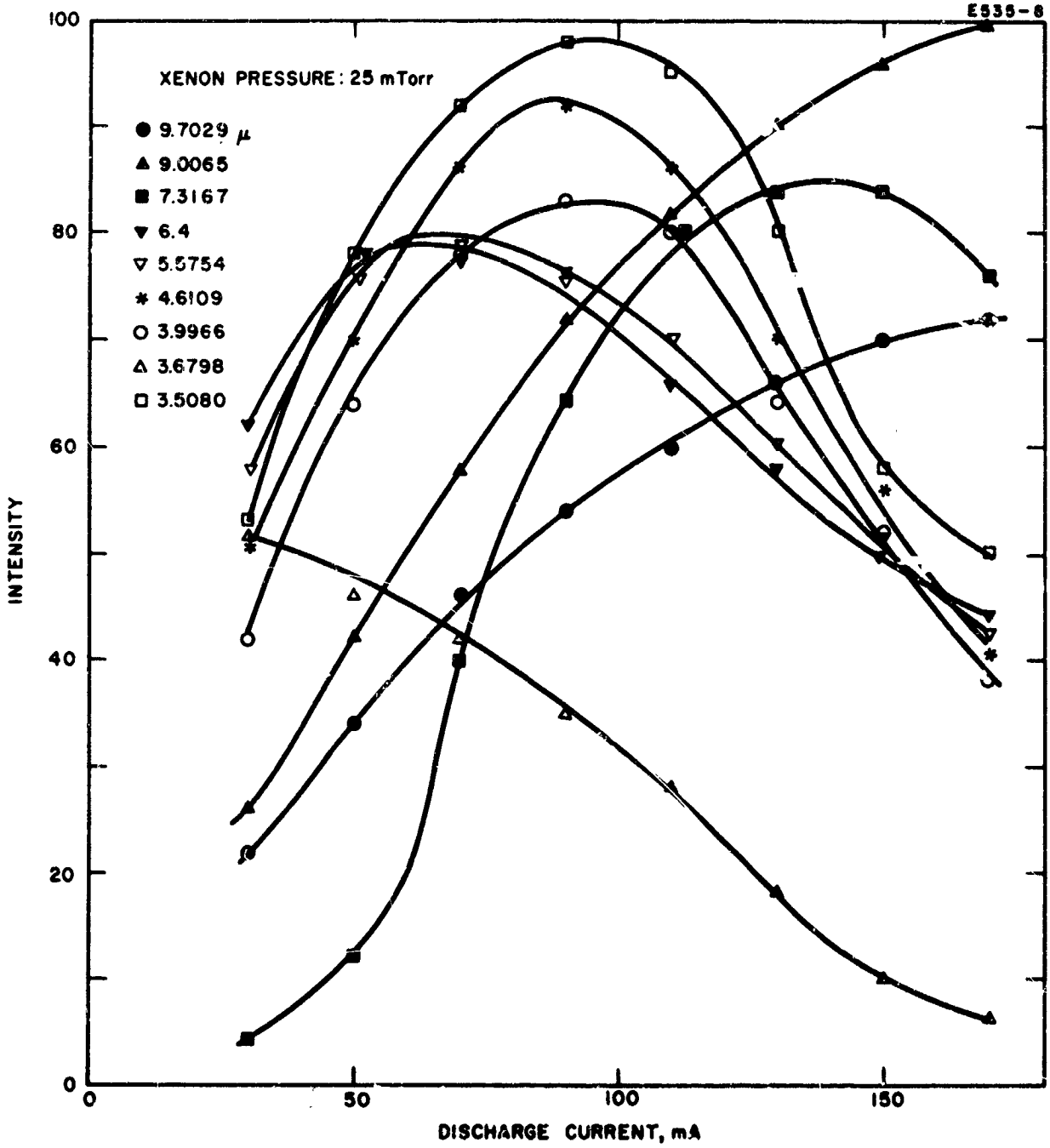

Fig. 17(a). Current variation of simultaneously oscillating laser transitions. Pressure 25 mTorr.

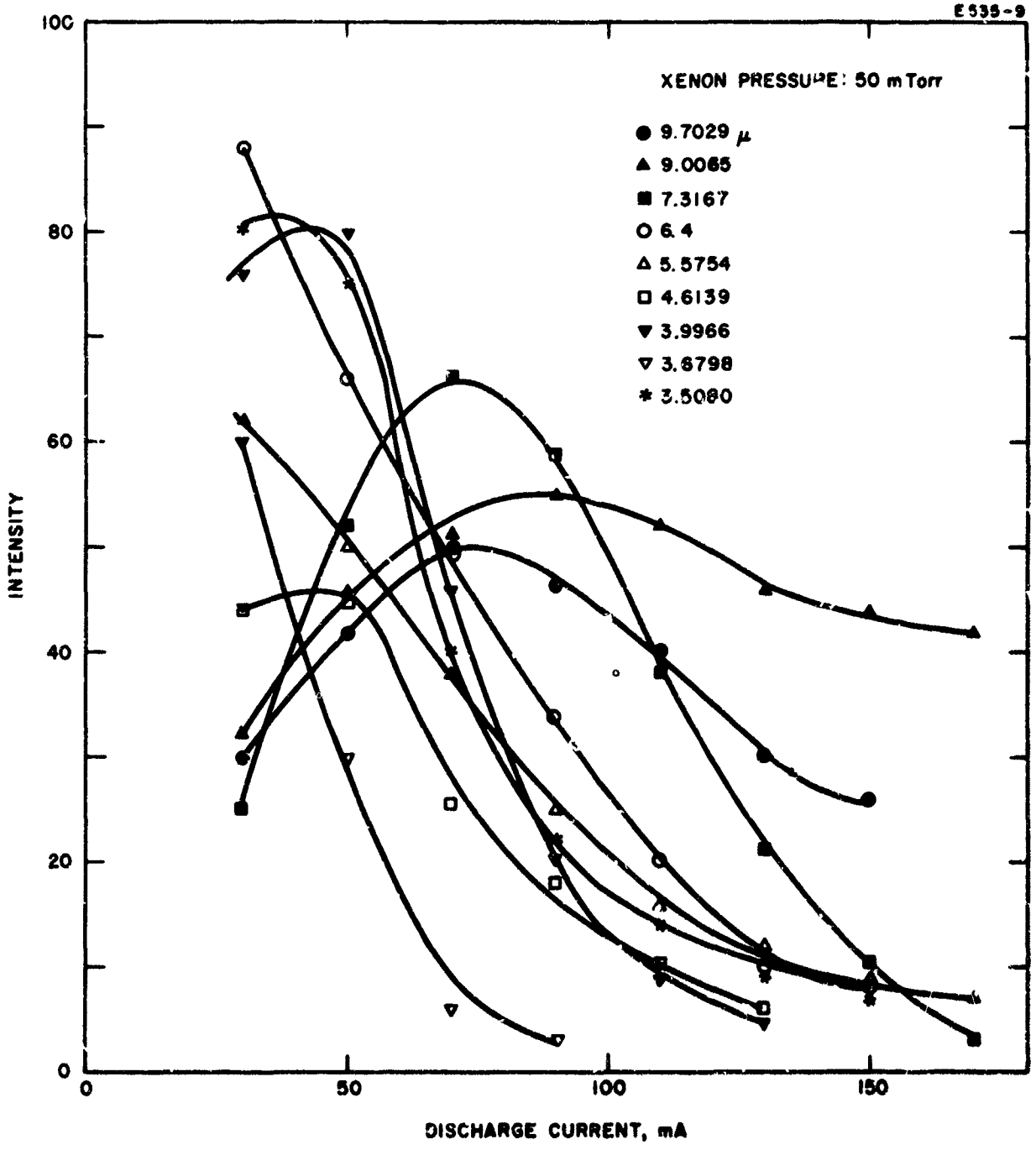

Fig. 17(b). Current variation of simultaneously oscillating laser transitions. Pressure 50 mTorr.

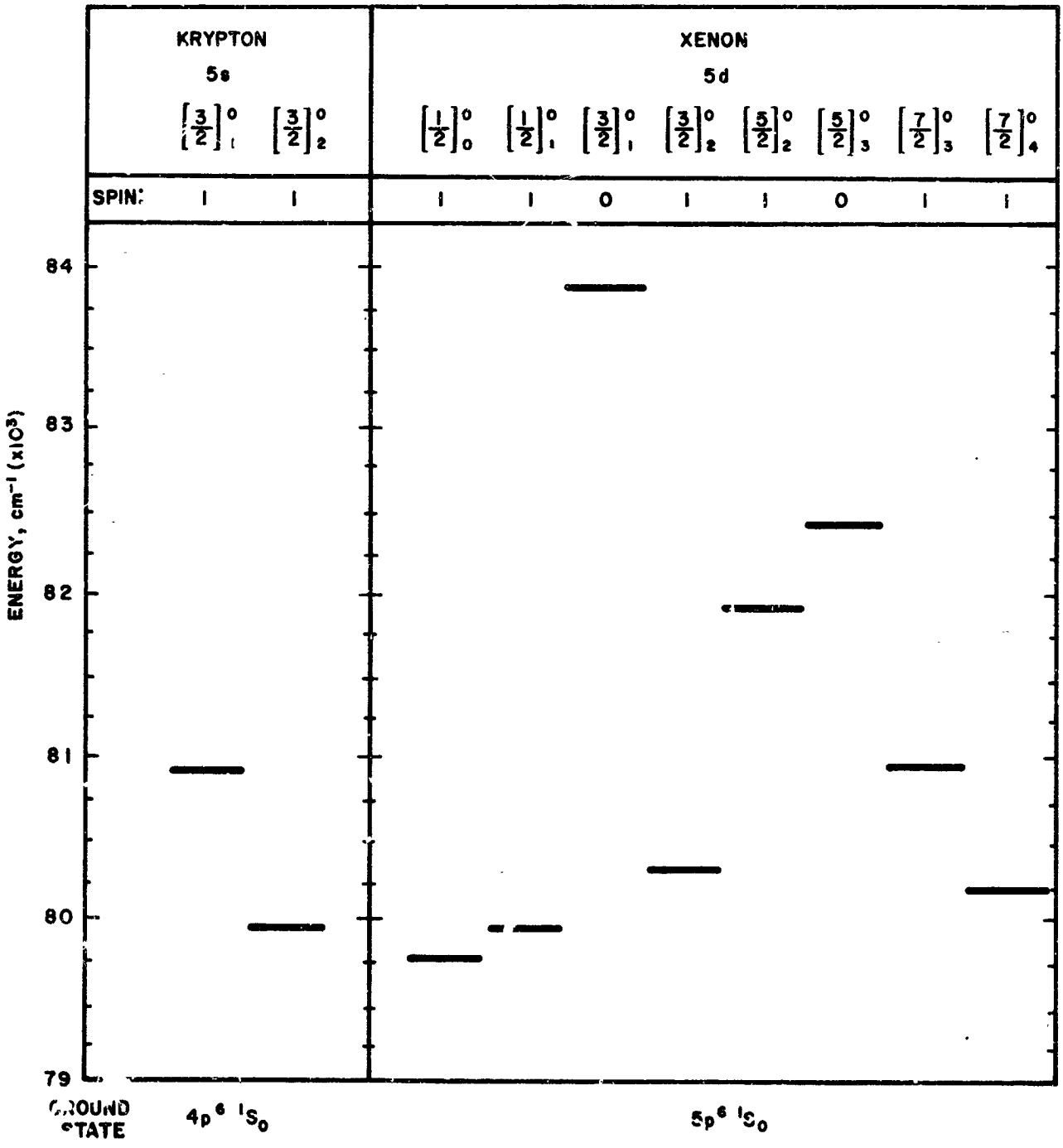

Fig. 18. 5d energy levels in xenon and 5s metastable energies in krypton.

F. Conclusions

Measurements of stimulated and amplified spontaneous infrared emission in the xenon discharge were made. Unamplified spontaneous radiation from the upper levels was too weak to be investigated. This indicates that these levels are only weakly pumped and explains why the power output is so low. The tremendous optical gain in many of the 5d-6p transitions results from the extremely long lifetimes and favorable branching ratios of the upper laser levels. A possible mechanism was postulated which explains the current dependence of the 5d-6p transitions. The xenon-krypton discharge was investigated as a system in which the upper laser levels would be selectively excited via collisions of the second kind with krypton metastables. No substantial increase in power output was observed.

BLANK PAGE

IV. SPECTROSCOPY OF THE PULSED XENON DISCHARGE

Pulse operation of the xenon laser was obtained with a 1 m long, 4 mm bore diameter discharge tube. The gas pressure was held constant at approximately 2.7 mTorr by trapping the xenon with liquid nitrogen. Input power to the discharge was provided by a Narda Microwave Corporation pulser capable of pulsing at a rate of up to several kilocycles; duration of the pulses was from 2 to 8 μsec. Maximum peak voltage and current were 15 kV and 30 A. The average output power was measured with the apparatus shown in Fig. 11. Output pulses at wavelengths less than 3.6 μ were observed by replacing the vacuum thermocouple and phase-locked detection system with an indium arsenide diode operated at room temperature. Output from the diode was displayed directly on a Model 551 Tektronix oscilloscope.

Wavelength scans of the average output power from the pulsed laser are shown in Figs. 19(a) and 19(b) for current discharge pulse lengths of 2 and 8 μsec, respectively. In both cases the peak current was 2 A and the duty cycle approximately 0.003. For both pulse lengths there is a significant variation between the pulsed output and the continuous wave output (see Fig. 16). The 2.6518 and 2.0268 μ transitions oscillated easily in the pulsed laser, but were difficult to observe in the cw laser. In addition, a line at about 1.7 μ appears in the pulsed output. This may be the $5d[3/2]^0_1$ - $6p[5/2]_2$ transition which has a wavelength of 1.7330 μ, a relative probability of 1/100 (Ref. 18), and a calculated relative line strength of 9 (refer to Table II).[20] There are also unidentified lines occurring during pulsed operation—at 8.4 (refer to Section III-D), 7.8, and 7.1 μ. The 7.8 μ line is fairly strong and the measurement accuracy was sufficient to determine that the 7.1 μ line is not the 7.3167 μ transition. Differences exist between the average output powers at the two pulse lengths. In particular, the 2.0268 μ line is stronger than the 3.5080 μ line when the discharge current pulse is 2 μsec long, but is weaker when the pulse duration is 8 μsec.

Figures 20(a) and 20(b) show oscilloscope traces of the shape of the output light pulses at 2.0268 and 3.5080 μ, respectively. For each case the evolution of the light pulse is shown as the current pulse length increases from 2 to 8 μsec. In each scan the upper trace is the current pulse, with a peak current of 20 A, and the lower trace is the light pulse. For all current pulse lengths, the output at 2.0268 μ is a sharply rising, rapidly decaying pulse with a width of less than 1 μsec. As the length of the current pulse increases, the amplitude of the 2.0268 μ output pulse decreases. This explains why, for a fixed duty cycle, the 2.0268 μ output is greater for the 2 μsec than for the 8 μsec current pulse (Figs. 19(a) and 19(b)). From Fig. 20(b) it is obvious that the structure of the 3.5080 μ light pulse is more complicated. With the shortest current pulse, the output laser pulse contains a small component generated during the current pulse and a larger component occurring

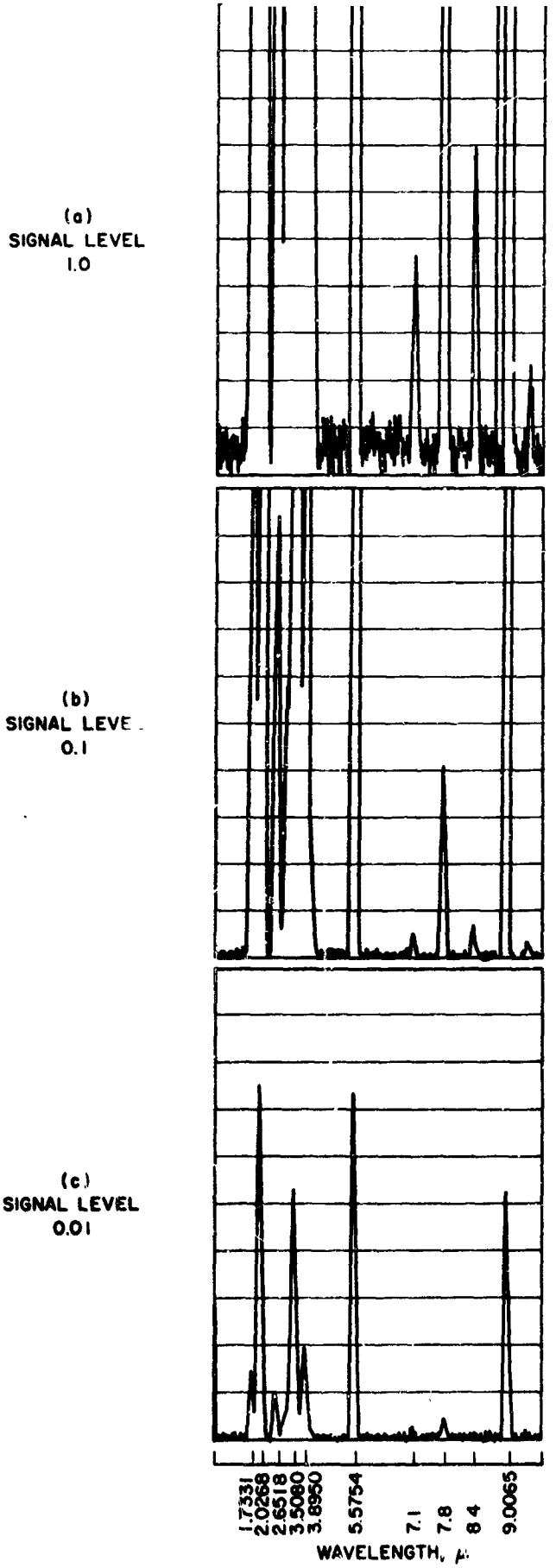

Fig. 19(a).
Wavelength scan from a pulsed xenon discharge. Current pulse length 2 μsec.

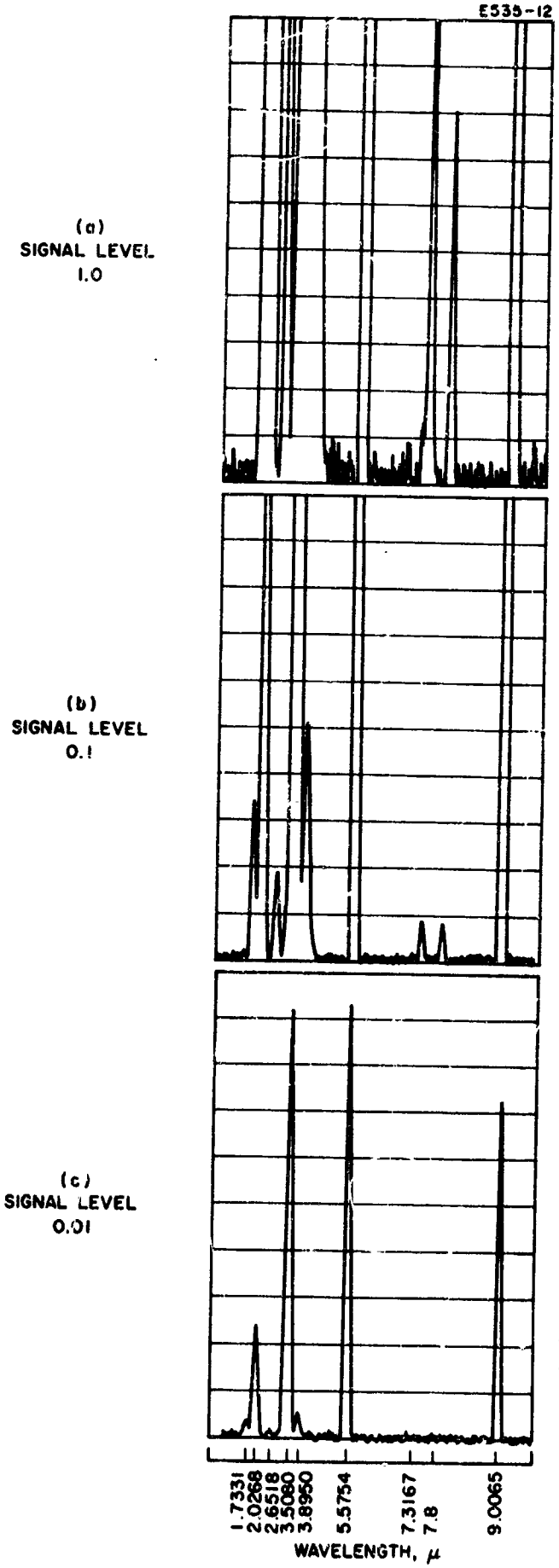

Fig. 19(b).
Wavelength scan from a pulsed xenon discharge. Current pulse length 8 μsec.

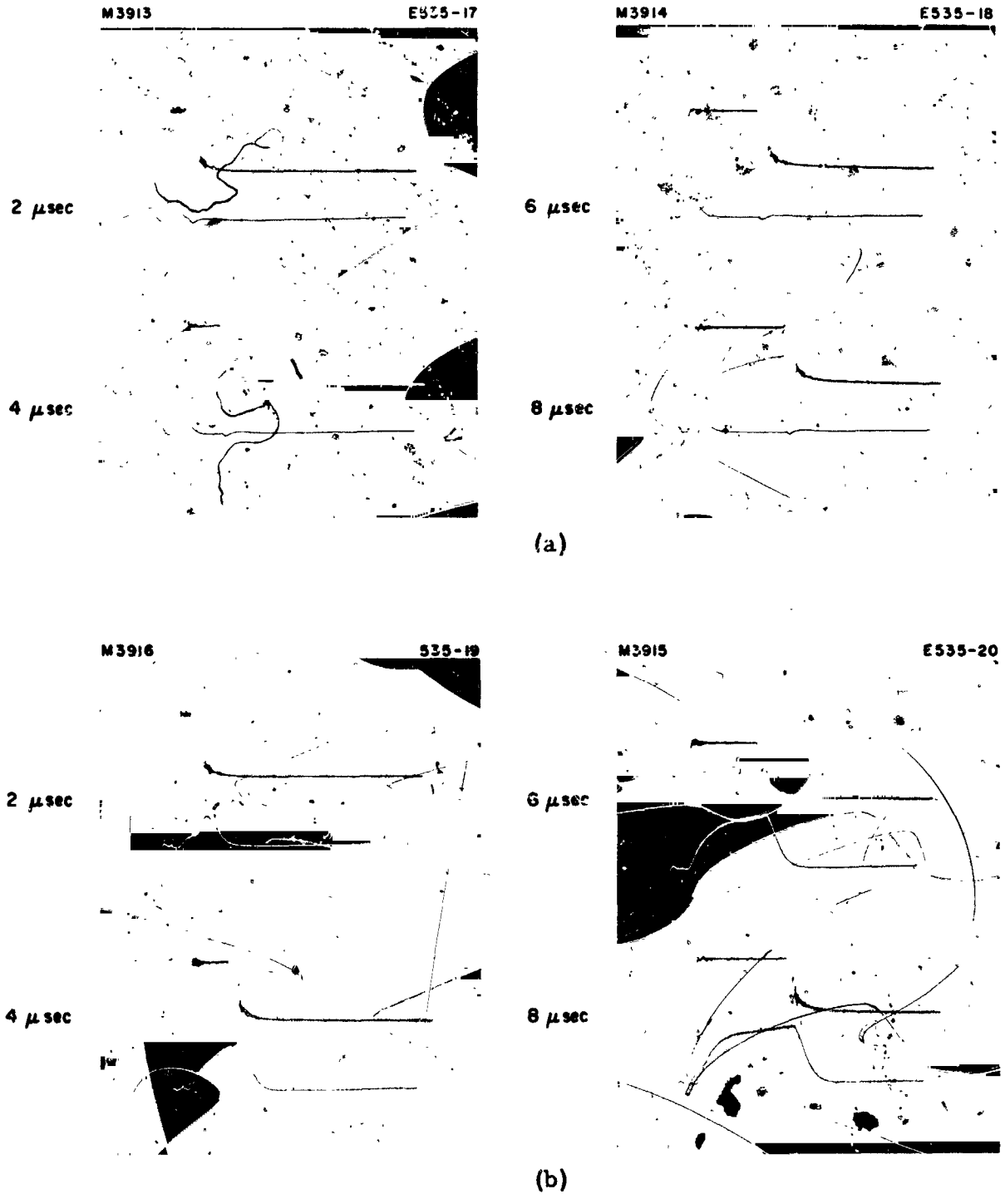

Fig. 20. (a) Laser pulses at 2.0268 μ. Discharge current pulses of 2, 4, 6, and 8 μsec duration. (b) Laser pulses at 3.5080 μ. Discharge current pulses of 2, 4, 6, and 8 μsec duration.

in the afterglow of the discharge. As the current pulse lengthens, the contribution from the afterglow increases only slightly while the light intensity produced during the current pulse increases rapidly and soon becomes the major portion of the total light output.

A possible interpretation of the pulse behavior is as follows. With short pulses the high electron energies lead to preferential excitation of the highest lying 5d levels. This results in maximum output in the 2.0268 μ transition originating in the $5d[3/2]_1^o$ level which has the highest energy (see Fig. 10). The 2.6518 and 1.7331 μ lines, which have the same $5d[3/2]_1^o$ upper level, also demonstrate the same higher output power at short current pulse behavior (Figs. 19(a) and 19(b)). As the electron temperature decreases in the afterglow of the short current pulse, the lower energy 5d levels are preferentially excited and the 3.5080 μ output increases. An additional factor affecting the short pulse behavior of the 2.0268 and 3.5080 μ transitions is that their estimated upper level life-times are 0.24 and 1.35 μsec, respectively.[19] Extension of this interpretation to the long pulse behavior is somewhat more tenuous. In this case the $5d[7/2]_3^o$ as well as the $5d[3/2]_1^o$ population has time to build up. In addition, the 6p levels are filled by means of cascade. Since the 2.0268 μ line oscillates only during the initial part of the current pulse, it is likely that the $6p[3/2]_1$ level becomes saturated; the $6p[5/2]_2$ level does not, however, and it allows the 3.5080 μ line to oscillate for the duration of the excitation pulse.

BLANK PAGE

V. NEW DISCHARGE CONFIGURATIONS

A. Introduction

Several new discharge configurations were designed with a view toward increasing the output power at 3.5080 μ. In each case, an attempt was made to produce an electron distribution which would selectively excite the upper laser level. One cold hollow cathode, two heated hollow cathodes, and a pentode discharge tube were constructed and investigated. In addition, a short internal mirror laser was fabricated to demonstrate the design of a simple, easily constructed laser utilizing the standard glow discharge.

B. Cold Hollow Cathode Discharge

In the negative glow region of the glow discharge,[23] the net charge density is such that the high energy electrons from the cathode (whose energies are approximately equal to the discharge striking voltage when the positive column is very short) either gain no energy or are actually slowed down. Thus a large number of relatively slow-moving electrons exist in this region and a great deal of excitation takes place there. The purpose of the hollow cathode discharge[24] is to provide a confined region of intense negative glow.

A cold hollow cathode discharge tube was constructed with three 10 cm long, 7 mm i.d. semicylindrical molybdenum cathodes. The anodes were molybdenum rods located in 4 mm wide slots on the extended circumference of the cathodes. A typical structure is shown in Fig. 21. The optical axis of the laser lay along the center of the cylindrical cathodes The tube was operated at xenon pressures up to 15 Torr and with cathode current densities of approximately 30 mA/cm^2. No optical gain at 3.5080 μ was observed. Under optimum operating conditions the discharge was blue, implying the presence of a high percentage of Xe II and Xe III. For stable operation the cold hollow cathode discharge tube required much higher input powers than those necessary for conventional dc-excited xenon glow discharges.

C. Heated Hollow Cathode Discharges

The presence of ion lines in the cold hollow cathode discharge indicated that the absence of gain at 3.5080 μ could be a result of electron energies which were much too high to excite the 5d energy levels in neutral xenon efficiently. Two heated hollow cathode discharge tubes were designed and constructed to provide lower energy electrons.

M 3884

Fig. 21. Anode-cathode configuration of the cold hollow cathode discharge tube.

The first tube was similar in design to the cold hollow cathode discharge tube. The oxide coated cathodes were indirectly heated by insulated heater wires arranged in slots along the outer surface of the cathodes. Platinum foil held the heater wires in place and acted as a heat shield. The heated hollow cathode discharge tube is shown in Fig. 22. In spite of the use of efficient cathode material, a prohibitively large amount of power was necessary to heat the cathodes to emitting temperatures. Since it was impossible to maintain a uniform discharge along an appreciable length of the laser, no conclusive determination of the presence or absence of optical gain at 3.5080 μ could be made.

In the second heated hollow cathode discharge tube (Fig. 23), five cylindrical cathodes and six ring anodes were aligned along the axis of the laser to provide a total discharge length of 52 cm The anodes were tungsten rings, 1/4 in. long and 1/2 in. in diameter. The cathodes were directly heated and were constructed by supporting a spiral of 5U4 cathode ribbon in a 2 in. long, 1/2 in. diameter ceramic-300 tube. Each cathode had 5-1/2 in. of active ribbon. The separation between each anode and the ends of the hollow cathodes was 1 in., and the cathodes were held by ceramic spacers in a 1-1/8 in. diameter tube. Total length of the laser was 72 cm. To maintain a common potential, the cathodes were heated in parallel. Since the resistance of the cathodes was comparable with that of the leads from the filament supply, it was necessary to ensure that all cathodes were maintained at the same temperature. The six discharges were driven in parallel from a common supply, and variable resistances were placed in each anode lead to provide a means for balancing the discharge currents. Careful adjustment of these balancing resistors resulted in a uniform discharge which was extremely intense along the axis and which diffused radially to fill the entire discharge tube. The striking voltage for the discharge was less than 25 V, and the required heater power was substantially less than that required by the indirectly heated hollow cathode discharge.

No laser oscillation at 3.5080 μ was observed with this discharge tube. In order to investigate the possibility of optical gain below the threshold for oscillation, the 3.5080 μ output from a small xenon laser was directed parallel to the axis of the heated hollow cathode discharge tube at several points along its diameter. No amplification was measured. An attempt was made to observe spontaneous emission in the hollow cathode discharge. However, in the 1 to 4 μ range — the wavelength region of interest — any existing infrared lines were of such low intensity that they were obscured by the thermal radiation of the cathodes.

M 3885

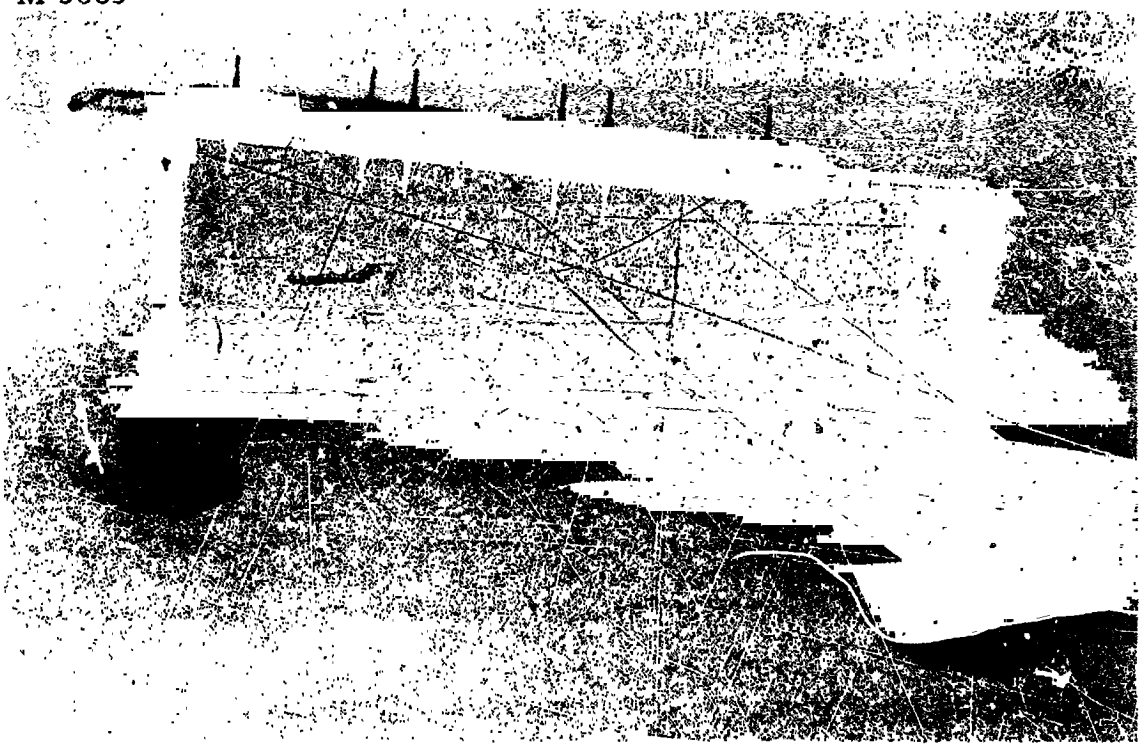

Fig. 22. Indirectly heated hollow cathode discharge tube.

M 3886

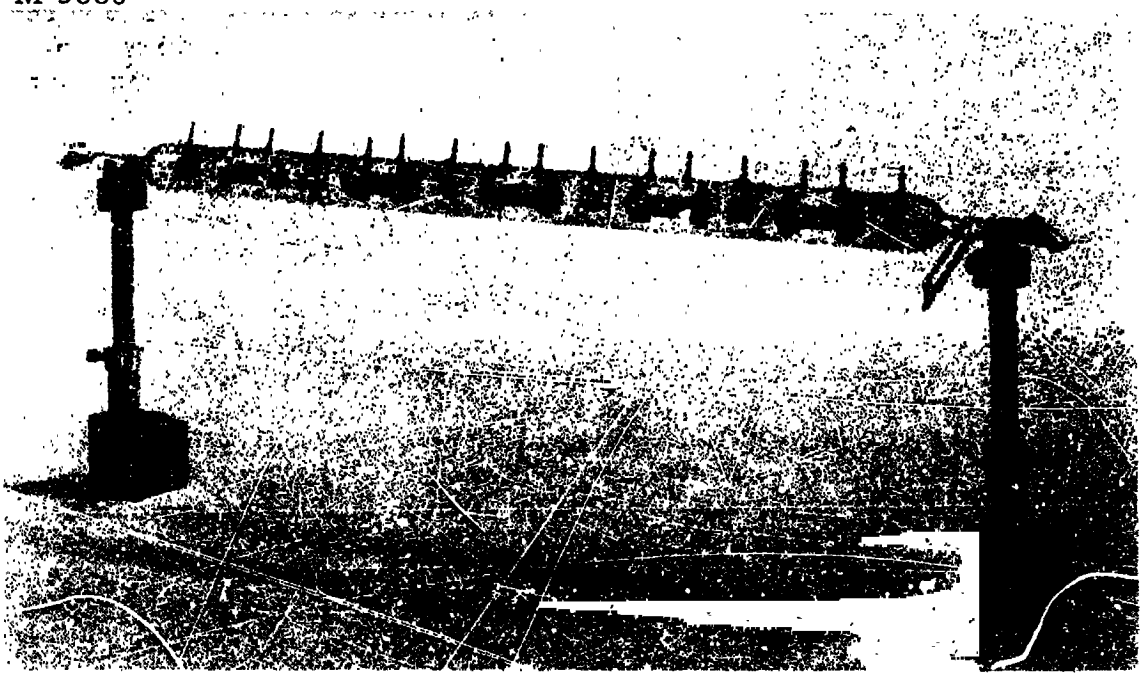

Fig. 23. Directly heated hollow cathode discharge tube.

D. Pentode Laser

Because the lower laser level of the 3.5080 μ line in xenon is not optically connected to the ground state, it exhibits a rather sharp electron excitation resonance below the excitation energy of the upper level. Thus, it appears that a beam of monoenergetic electrons of the proper energy could be used to excite xenon atoms selectively to the upper laser level. Two experimental approaches were undertaken to examine the potential of this concept. The hollow cathode technique, which is discussed elsewhere, would provide a source of monoenergetic electrons but lacks the continuous control of that energy and is therefore not a useful tool for detailed examination of the processes involved; this would probably provide the more practical laser configuration, however.

In this proposed experimental device, it was considered necessary to make provision for monoenergetic electrons of variable energy in the range of the upper levels of the near infrared laser lines in neon and xenon. The tube would also necessarily remain attached to a pumping station and manifold to allow ease of pressure variation and exchange of gases. A similar experiment performed at Bell Telephone Laboratories[25] provided a logical starting point for our investigations. In the BTL experiment a triode arrangement was used with the equipotential region extending from the extraction grid to the anode; in this region laser action occurred. The three-electrode structure suffers some lack of versatility since a variation in the grid voltage creates two simultaneous effects — variation in electron current density (although this may be small in the temperature limited condition) and change of electron energy in the equipotential region. The results of these simultaneous variations might be difficult to unscramble.

To eliminate this uncertainty we built a pentode structure (see Fig. 24) with two connected grids defining the equipotential region, neither of which served as either the anode or as the extraction grid. Thus, the changes in the electron current density could be effected with no change in electron energy in the equipotential region, and vice-versa.

Because the triode tube had been successful (since oscillation had been observed in the 2.026 μ line of xenon and the 1.152 μ line of neon), it was decided to follow its design, other than the change mentioned. The emitting length was just over 19 cm, the width 4 mm, and the distance between extracting grid and cathode was to have been 1/2 mm. This would then have delivered an electron current on the order of 600 mA with 30 V difference between the cathode and the first grid. The cathode was indirectly heated to eliminate a potential drop along its length. The equipotential region provided a 3 mm diameter circular cross section for passage of the laser radiation.

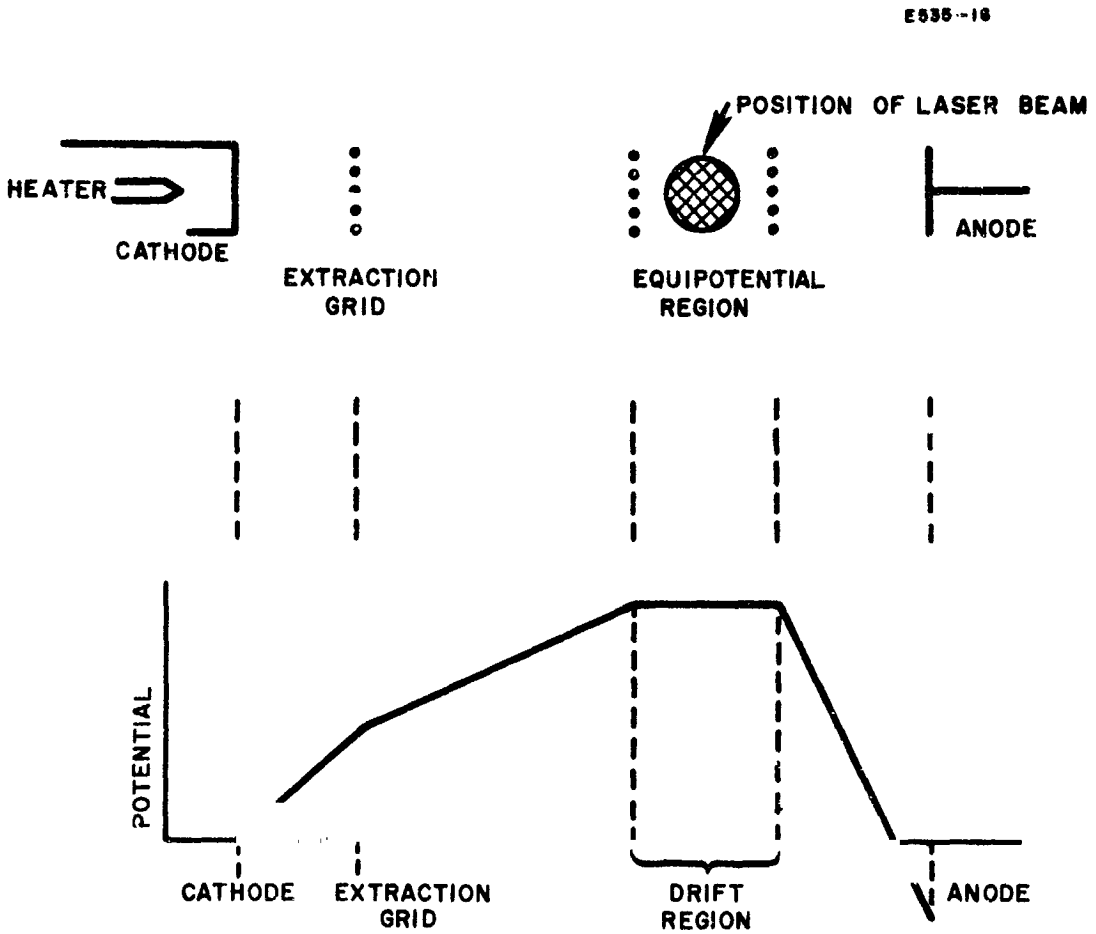

Fig. 24. Electrode arrangement and potential diagram of the pentode laser.

Construction of the pentode structure proved more difficult than anticipated, particularly in maintaining the grid cathode spacing accurately enough to eliminate large variations in current density along the length as a result of its $1/d^2$ dependence. Partly to assure greater uniformity of current density and partly because of practical construction difficulties, the cathode grid spacing was extended to 1 mm, in the hope that the same current density could be drawn at higher voltages. Measurements of this distance performed after conclusion of the experiment showed that this critical spacing ranged from about 1.7 mm to 3.5 mm with the central 60% of the length being fairly constant at 1.7 mm (about 20% on each end warped badly). To reduce warping, boron nitride support rings were placed about every 3.75 cm (see Fig. 25), but they proved inadequate to perform their anticipate l function. Inclusion of the boron nitride spacers (each 1-1/2 mm thick) also reduced the emitting area slightly so that the actual area of fairly uniform, and unblocked emission was reduced to about 50% of its original design value.

The BTL experiment again provided a lead in establishing the pressure range of interest. They had measured appreciable gain of the 1.152 μ line in neon at pressures around 1 Torr. Our own search for oscillation at this frequency was conducted in this pressure range, but with negative results; no measurement of the single pass gain was attempted.

While no mention of the 3.508 μ line of xenon was made by the BTL workers, they did observe oscillation of the 2.026 μ line at a pressure of 37 mTorr. Again, this is the region in which our investigation began, varying the pressure by about an order of magnitude in either direction. No detectable infrared laser power appeared over the entire range. Since we are primarily interested in the very high gain line at 3.508 μ, a short oscillator was built and packaged to provide a convenient source for the measurement of single pass gain in the pentode laser. No detectable gain appeared over the entire pressure range.

It is not surprising that no oscillation was observed in the pentode laser. With the active length of the laser cut nearly in half by cathode warpage it is not difficult to surmise that the losses might exceed the gains and destroy the necessary condition for oscillation. It is more difficult to explain our failure to observe any single pass gain at 3.508 μ. Again, the gain would be reduced by a factor of two below that of a pentode built according to our original design, but it should still be measurable. It might also be reduced by electron current densities below those anticipated, but this should not have been as much as an order of magnitude and should have left a measurable residue of gain.

Considering the difficulties encountered in construction and operation, and on the negative results achieved, there seems to be little point in considering future generations of pentode lasers.

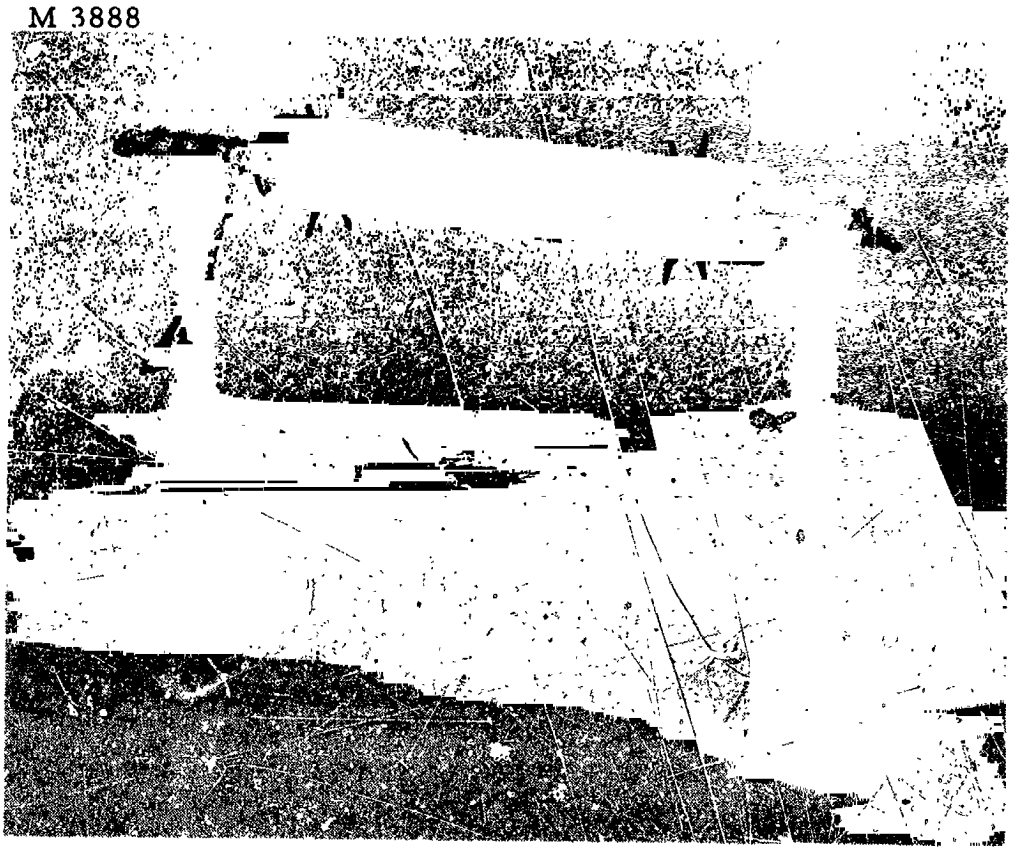

Fig. 25. Pentode laser.

E. "Ball-Socket" Laser

A small, efficient xenon laser with internal mirrors was designed and built for use with a conventional dc discharge. The laser, which was operated successfully, is shown in Fig. 26. The internal mirrors were a quartz flat and an aluminized mirror fastened directly on the ends of the discharge tube. This eliminated the Brewster angle windows. Adjustment of the mirrors was provided by putting a ball-socket joint near the end of the tube supporting the spherical mirror. The vacuum seal was sufficiently tight that at 10^{-7} mTorr the mirror could be freely moved without an increase in pressure. In spite of the low Fresnel reflection coefficient of the quartz window, the gain of the 3.5080 μ transition is sufficiently high to allow oscillation in the 15 cm long, 2 mm i.d. discharge. It was impossible to discriminate between superradiant and laser output; the great sensitivity of the output to mirror adjustment, however, indicated that a large portion of the output was laser radiation. A higher power laser with less superradiant output could be constructed by replacing the quartz flat with a germanium flat (reflectance $\simeq$ 36%, transmittance $\simeq$ 50%).

F. Conclusions

Several new discharge configurations were investigated for use as high power 3.5080 μ xenon lasers. All of the candidates required much larger total amounts of input power than the normal glow discharge, and none of the new configurations produced any output or optical gain at 3.5080 μ. The high gain of the xenon flow discharge led to the construction of a very simple and efficient internal mirror laser.

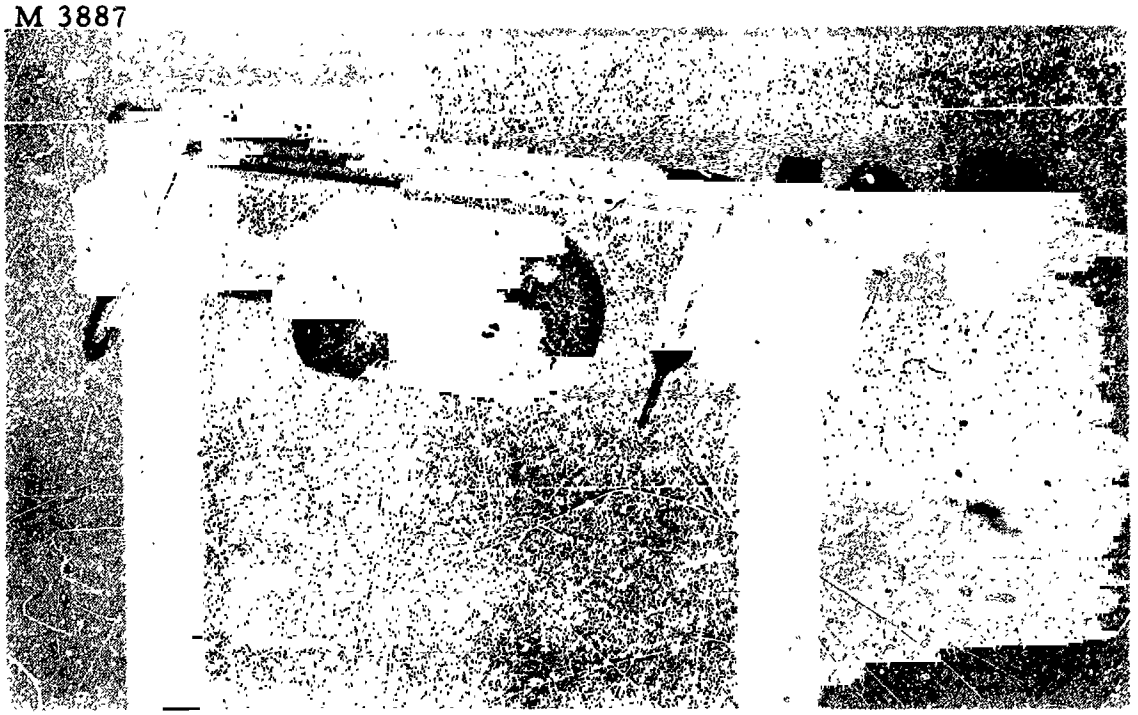

Fig. 26. A short, internal mirror xenon laser which uses a ball-socket joint for adjustment of its mirrors.

BLANK PAGE

VI. ELECTRON ENERGY SPECTRA IN GAS LASER DISCHARGES

A. Introduction

In gas laser discharges the rate of production of excited atoms or ions $r(cm^{-3}\ sec^{-1})$ is the product of three factors: (1) the density of ground state atoms n/cm^3; (2) the cross section for the process $\sigma(cm^2)$; and (3) the amount of electron flux per unit energy available for the process. This last quantity is also called the electron energy spectral intensity $S(cm^{-2}\ sec^{-1}\ eV^{-1})$ and is defined by eq. (10). Equations (8) and (9) are functions of the electron energy ϵ(eV), and the resultant rate is, by definition of S,

$$r = n \int_0^\infty \sigma(\epsilon) S(\epsilon) d\epsilon \quad . \tag{7}$$

The density n is known from the gas pressure. Experimental determinations of σ are available for helium and to some extent for neon; good theoretical estimates are possible and have been reported for the more important transitions and for the heavier noble gas atoms.[26] We present measurements of the function $S(\epsilon)$ as it develops in gas laser discharges. The measurements were taken with a recently developed electron energy spectrometer. The results are described first, and the experimental procedure and the limitations are discussed in the section on instrumentation.

B. Experimental Results

Typical results are shown in Figs. 27 and 28, where six examples of measured energy spectra are plotted (three for helium-neon and two for xenon discharges, respectively). All are for 7 mm bore tubes. Since the spectral values $S(\epsilon)$ are exactly proportional to the discharge current over a large range, we chose the same discharge current density ($0.1\ A/cm^2$) for all six cases. In order to improve the presentation, however, the curves in Fig. 27 were shifted vertically by individual factors, as indicated.

For each of the helium-neon spectra of Fig. 27, we show by a dotted line a Maxwellian spectrum $S(\epsilon)$ proportional to $\epsilon[\exp(-\epsilon/kT)]$ of the temperature which matches the low energy portion of the measured spectrum. The value of the temperature for the Maxwellian is shown for each case. For all values of Rp the low energy portion of the spectrum is well approximated by Maxwellian. For the small Rp value (curve A), even the fast portion of $S(\epsilon)$ is generally in agreement with the Maxwellian spectrum. As the Rp value or the gas pressure is increased,

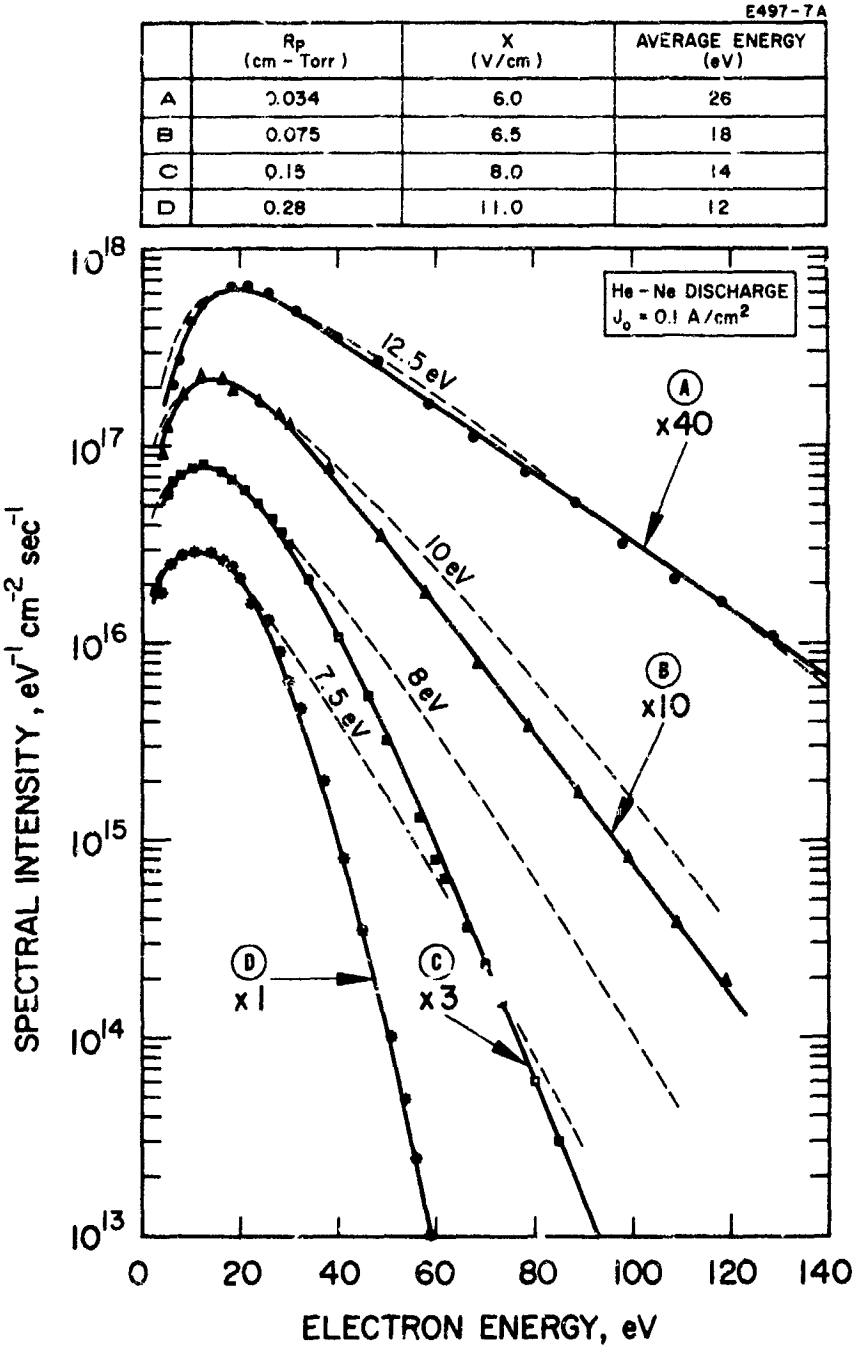

Fig. 27. Electron energy spectra in helium-neon gas laser discharges.

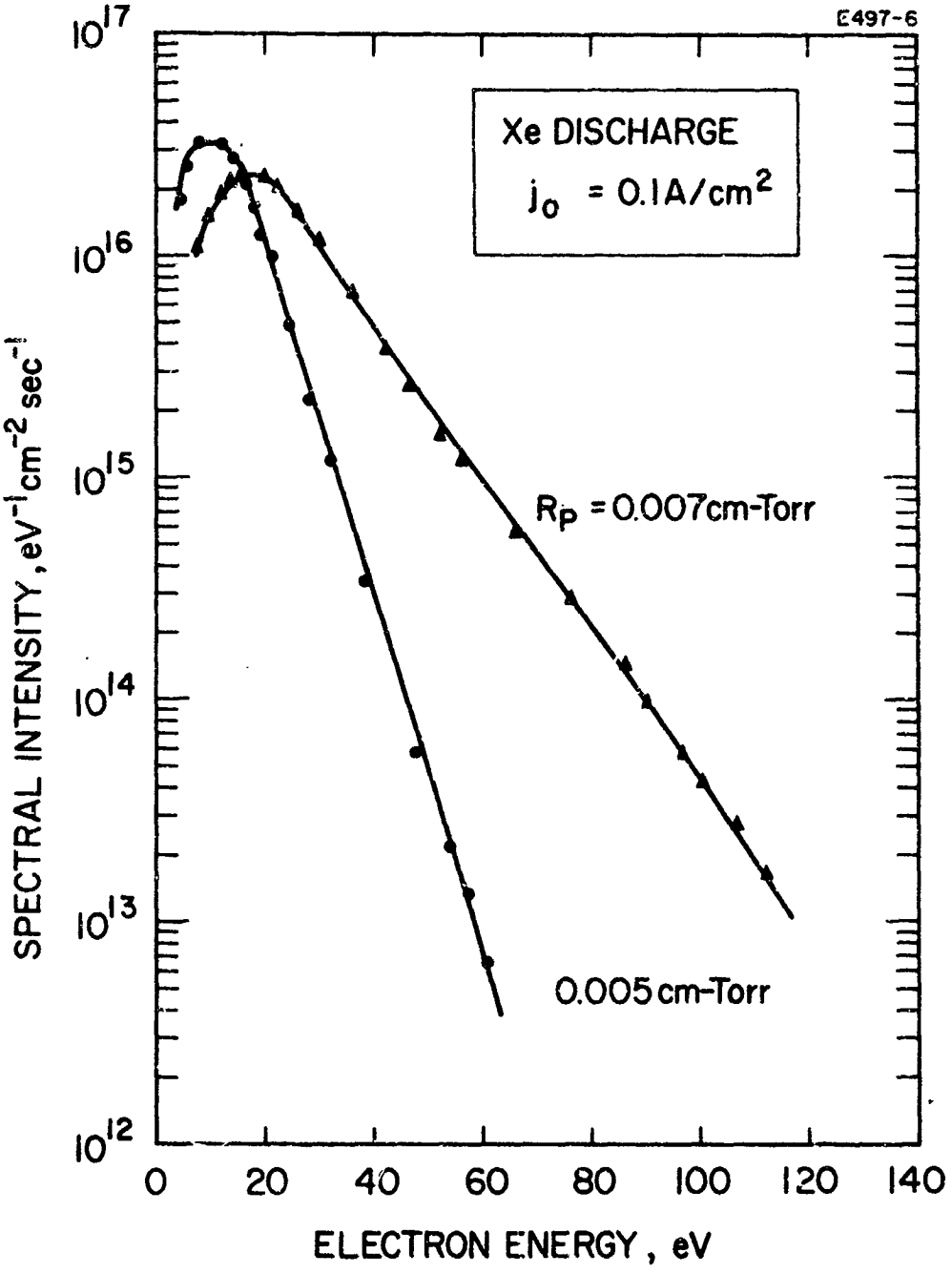

Fig. 28. Electron energy spectra in xenon gas laser discharges.

however, this agreement fails and the relative population of high energy electrons decreases more rapidly than the matching Maxwellian. For example, the measured spectral intensity at 60 eV for Rp = 0.28 Torr cm is about two orders of magnitude smaller than the corresponding value of the Maxwellian. In general, the energetic part of these measured curves at higher gas pressures is well represented by an exponential function. Approximation of this part by another Maxwellian function leads to the assignment of a tail temperature, which represents a lower value than the one which characterizes the bulk of slower electrons.

In xenon discharges, we have observed the onset of strong oscillation and the appearance of moving striation for Rp values above 0.06 Torr cm. The accurate measurement of the spectral intensity at large values of Rp was impossible.

As an example of the use of the spectrum marked C in Fig. 27, we compute the generation rate r of helium ions using the known cross section data.[27] We find the integral eq. (7) to yield $r/n = 12\,\text{sec}^{-1}$. For the 7 mm bore tubing at pR = 0.21 Torr cm, $n = 1.6 \times 10^{16}/\text{cm}^3$ and $r = 7.1 \times 10^{16}/\text{cm}^3/\text{sec}$. Since volume recombination is negligible, all ions produced go to the wall. With the volume to surface ratio 0.5R, the wall ion current density is

$$j_i = \frac{1}{2}\, eRr \quad , \tag{8}$$

or 2.5 mA/cm^2. We now consider the power balance and neglect the radiative part. Each ion transfers its kinetic energy (which it gains during its acceleration toward the wall) in an amount equal to the ionization potential to the wall. Because of the current balance, an identical electron current density arrives and delivers a power determined by the average kinetic electron energy E_e. The power density received by the wall is $J_i(E_i + E_e + 24.6)$. On the other hand, the power supply feeds $X j_o (\text{W/cm}^3)$ into the discharge volume, where j_o is the discharge current density and X the electric field in the column (e.g., for curve C of Fig. 27, $X j_o = 0.8\ \text{W/cm}^3$). Thus, with

$$X j_o = er(E_i + E_e + 24.6) \tag{9}$$

and with the value r/n determined above, we find the average energy $E_i + E_e$ is approximately 30 eV. This rather rough estimate gives a reasonable value for the sum of the ion and electron energies at the wall.

C. Instrumentation

The classical method for measuring electron energy spectra is the Langmuir probe technique. Because of its limitations and interpretational uncertainties[28] we used the instrument shown in Fig. 29 (see Ref. 29). The electrons are extracted through a small hole in the anode, and their energy is then measured in high vacuum by an energy analyzer.* This method produces more accuracy in the energetic part of the spectrum and causes less disturbance of the plasma at the position of the probing hole. An extraction system of the triode type, used in this application, is shown in the enlarged insert of Fig. 29. G_1 and G_2 consist of apertures 0.5 mm thick, with 1 mm bore and spaced by 0.5 mm thick insulators. The assembly is brazed into a molybdenum plug and the drilling is done after the braze in order to ensure concentricity. After careful electron-optical alignment we take recordings of collector current versus selector potential, reduce them to flux density (knowing the hole area), and carry out the differentiation with respect to voltage.

It is important to note that the $S(\epsilon)$ as introduced in eq. (7) is the true spectral intensity of the electrons in the discharge and is defined by

$$S(\epsilon) = \eta \epsilon^{1/2} F(\epsilon) \tag{10}$$

where $\eta \epsilon^{1/2}$ is the velocity equivalent of ϵ (cm/sec) and $F(\epsilon)$ the distribution function (per cm^3/eV). The spectral intensity measured at the extraction hole $S_m(\epsilon)$ is closely related to $S(\epsilon)$. A completely anistotropic distribution in which all electrons go in one direction, e.g., along the axis of the tube, is correctly measured by the flux through a hole whose plane is perpendicular to the axis. For a distribution which is perfectly isotropic, $S_m(\epsilon) = 1/4\, S(\epsilon)/4$, and the orientation of the hole is irrelevant. The discharge which we consider here has a nearly isotropic electron velocity distribution.

*The percentage of the electrons which make elastic collisions after passage of the hole can easily be estimated. At the highest pressures and for the largest holes used it is 5%, with less than 2% for inelastic collisions.

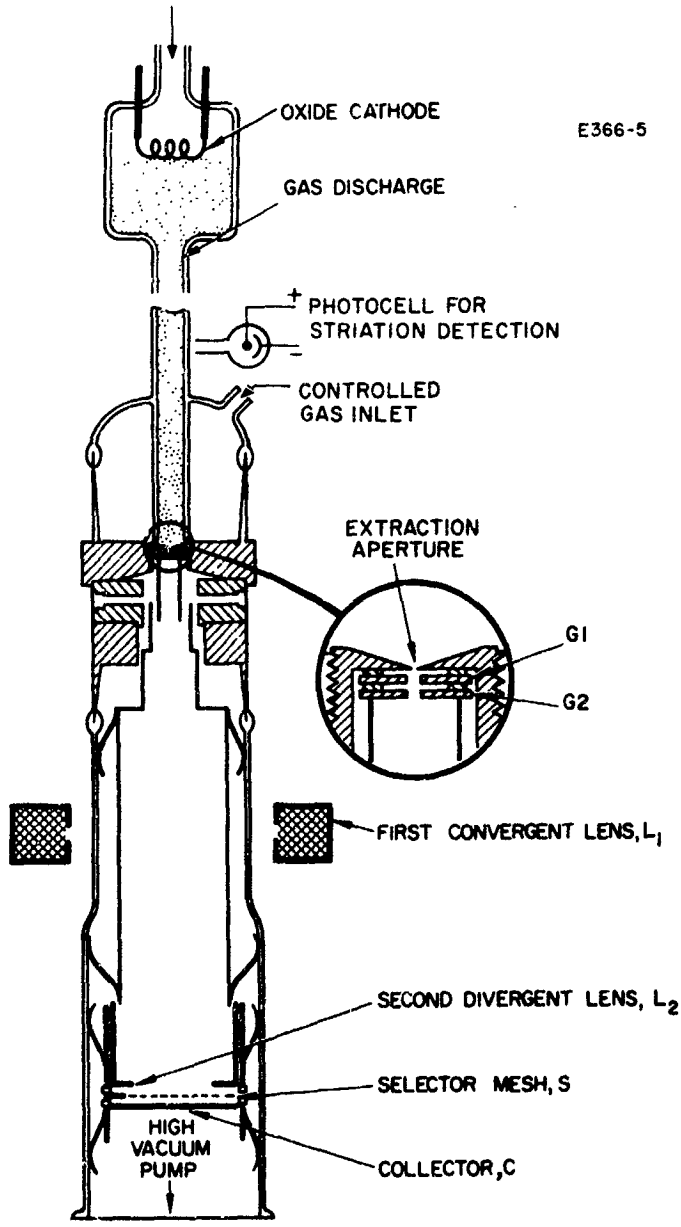

Fig. 29. The Heil electron energy spectrometer attached to the anode of a gas laser discharge.

D. Theoretical Determination of the Electron Energy Distribution

Consider a thin disk across the tube to be the volume element; the distribution function F is an average over such an element. Since there is a radial variation of the plasma potential, a radially moving electron continuously changes kinetic energy into potential energy and vice versa. The function F defined here implies a distribution in and an average over the kinetic energy only. Then F is independent of time and position. The angular dependence is summarily described by the main axial spectrum $S(\epsilon) = \eta\epsilon^{1/2} F(\epsilon)$ and the small radial spectrum $a(\epsilon) S(\epsilon)$, where $a(\epsilon)$ is defined as the ratio between the radial current density to the wall and the average axial current density in the discharge tube. This ratio is typically of the order of a few percent. Following the procedure of Druyvesteyn, Smit, and others,[30] we list the following processes which determine F:

1. electron-electron collisions
2. elastic electron-atom or -ion collisions
3. the electric field $- X\eta\epsilon^{1/2} \, dF/d\epsilon$
4. inelastic electron atom collisions $- n_o \sum_\nu \sigma_\nu \eta\epsilon^{1/2} F$
5. wall collisions $- 2/R \, a(\epsilon)\eta\epsilon \, F$.

Processes (1) and (2) are quite negligible; process (5) is new and turns out to be dominating in typical laser discharges. In the energetic part, which interests us most, processes (4) and (5) are loss terms, and (3) is the only production process (production resulting from process (4) is unimportant because the energy thresholds ϵ_ν are large compared with the tail temperatures). From processes (3), (4), and (5) we derive the energy distribution function

$$F(\epsilon) \propto \exp\left(- \frac{2a}{RX} \epsilon - \frac{n_o}{X} \sum_\nu \int_{\epsilon_\nu}^{\epsilon} \sigma_\nu(\epsilon') \, d\epsilon'\right) . \qquad (11)$$

The second term in the exponent can be determined from the data for helium and neon.

At electron energies below the threshold ϵ_ν and at low gas pressures, only the first term in the exponent is finite, and it is linear in ϵ. The effect of the second term becomes important for relatively high gas pressures and for energies well above the threshold ϵ_ν. It rises first quadratically above the threshold but then gradually changes into a linear function of ϵ above 50 eV (for neon and helium). The electron

temperature of the slower electrons ($\epsilon < \epsilon_v$) is, therefore, roughly equal to RX/2a, whereas the fast tail temperature is related to the combination of the two terms representing the wall losses and the inelastic electron-atom collisions. The a-value determined from the measured spectral intensity and from the ion generation rate, using eq. (7), are in reasonable agreement.

E. Conclusions

Absolute measurements of the electron energy spectrum in helium-neon and xenon gas laser discharges have been obtained. The electron energy distribution is nearly Maxwellian for small values of Rp (a product of the radius and the pressure) but deviates strongly from the Maxwellian for larger Rp's. The plasma boundary (wall) effect and the electron-neutral inelastic collisions are of dominant importance in forming the electron energy distribution in laser discharges; their effects have been theoretically formulated from a simple consideration of the energy conservation. The theory explains the observed dependence of the electron energy distribution as a function of Rp. The experimental results are in reasonable agreement with this theory.

We hope that the better knowledge of the electron energy distribution function and the processes which determine its shape will limit the range of speculation about the many unknown processes active in gaseous lasers.[31, 32] For the helium-neon laser discharges, we can say specifically that the direct deexcitation of helium metastables by slow electrons is totally negligible; also, the electron excitation of excited (metastable) atoms is negligible. Processes involving slow electrons generally can be excluded because there are few such electrons.

VII. SUMMARY

Although each section of this report includes a detailed summary and analysis of the results of the various experiments, all the conclusions are briefly summarized in this section so that an over-all view of the program accomplishments may be obtained.

- Extremely high small signal gains at 3.5080 μ were measured in pure xenon dc-excited discharges. The maximum observed gain was 70 dB/m. Over the range of xenon pressures (10 to 150 m Torr) and tube diameters (2.6 to 8 mm) investigated, the small signal gain increased monotonically as gas pressure and tube diameter decreased. The experimental results indicated an approximate $pd^3 = C$ relation, where p is the xenon pressure, d is the amplifier bore diameter, and C is a constant depending (in an inverse fashion) on the gain.

- Regardless of the operating parameters, gain saturation occurred at low input signal levels. This sets a limit on the power output from a 50 cm long laser of 10^{-3} to 10^{-4} W. This prediction of low output power at 3.5080 μ from xenon oscillators based on the observation of low saturation power was verified by experiment. In spite of the low power requirements of the discharge, the small amount of output power available at 3.5080 μ leads to efficiencies of the order of 10^{-2} to 10^{-3}%. In multi-transverse mode lasers, there was little variation of efficiency with tube diameter and gas pressure. However, for lasers oscillating in one or only a few low order transverse modes, the efficiency decreased as the bore diameter increased.

- Infrared spontaneous emission from the dc-excited xenon discharge was too weak to be measured. This indicated that the levels in the discharge are only weakly pumped and helps to explain why the available output power is so low. The tremendous optical gain present in many of the 5d-6p transitions is presumed to result from the extremely long lifetimes of the upper levels and favorable branching ratios.

- The current and pressure dependence of amplified spontaneous emission was investigated for several infrared lines. The results of these measurements, as well as similar observations at many laser frequencies, formed the basis for a tentative explanation of the current dependence of the gain and output power on the 5d-6p laser transitions.

- A laser capable of oscillating at wavelengths up to 15 μ was constructed with sodium chloride Brewster angle windows and external mirrors. The observation of 1/2 mW of output power at 9.0065 μ from this laser (50 cm long) is the first measurement of significant cw power at a wavelength so far into the infrared. In addition this laser oscillated at two wavelengths previously unobserved, 6.4 and 8.2 μ.

- Selective excitation of the 5d levels in xenon may occur by means of collisions of the second kind with the 5s metastable levels of krypton in a xenon-krypton laser discharge. Measurements performed failed to indicate a significant increase in output power from the xenon-krypton laser on any of the 5d-6p transitions.

- Observations made with a pulsed xenon laser indicated that in the pulsed mode of operation there was a definite variation in the manner in which the different 5d-6p laser transitions occur. A tentative observation was offered for the observed phenomena. Laser action was observed for the first time at 1.7331 μ.

- Several new discharge configurations were designed and constructed. These included three hollow cathode discharge tubes — one cold, one indirectly heated, and one directly heated — and a pentode laser. None of these lasers produced measurable output power or gain at 3.5080 μ. In addition, each of these tubes required, for stable operation, an input power of at least a factor of 10 greater than a glow discharge tube of comparable size. On the basis of these experiments, the standard dc-excited glow discharge is the most effective and efficient gas laser discharge.

- Measurements of electron energy spectra indicated that in helium-neon and gas laser discharges, the electron energy distributions deviate strongly from the Maxwellian function. Although the "fail temperatures" of energetic electrons agree approximately with values obtained by microwave measurements, the average energy is larger. The number of slow electrons was found to be less than that for the Maxwellian distribution, and the dominant factor in the formation of the spectra was the electron wall collisions.

VIII. DEVICE TO BE DELIVERED

As a result of discussions with Willard Wells and Jack Siddoway of the Jet Propulsion Laboratory, it was decided that delivery of a multi-wavelength infrared xenon laser would satisfy the objectives of the program. In addition, emphasis would be placed on enhancing the output power at 9.0065 μ.

Construction of the laser has been completed. The discharge tube is 75 cm long and 8 mm i.d., the package length is approximately 95 cm. The laser is provided with sodium chloride Brewster angle windows and a germanium output mirror. Such an arrangement allows simultaneous oscillation at many infrared wavelengths. Power output at 9.0065 μ of greater than 1/4 mW is expected. In addition, a new mirror configuration using two quartz mirrors, one with a small output coupling aperture, is being investigated as a means of enhancing the 9.0065 μ radiation and suppressing all other wavelengths.

BLANK PAGE

APPENDIX I – COLLISIONS OUTSIDE THE HOLE

In order to estimate the influence upon the S-values of collisions after the electrons have left the hole, we list the following possibilities for distortion of the energy spectrum:

1. An electron makes an inelastic collision with a gas atom. Because of such collisions

   a. the low energy S-values are increased and extended to lower values than would be possible in the plasma

   b. the high energy S-values are reduced.

2. An electron makes an elastic collision with a gas atom. Because of such collisions, the electron is thrown out of the range of the optical path. Considering the small aperture used in the optical system, it probably will not reach the collector. A small, uniform reduction in the S-values is to be expected.

We now estimate the gas density decrease away from the hole. The gas kinetic cross sections which are shown in Fig. 30 are such that atom-atom mean free paths are larger than the hole. Therefore, we have essentially Knudsen (collisionless) flow, which means that the density $n(r)$ decreases quadratically from the initial value n_o at the hole (radius r_o)

$$n(r) = \left(\frac{r_o}{r}\right)^2 n_o \quad . \tag{I-1}$$

The probability for a collision (cross section σ) along the path element dr is $n(r)\sigma dr$. The electron on its travel from $r = r_o$ to $r = \infty$ has a collision probability of

$$\int_{r_o}^{\infty} n(r)\,\sigma dr = \sigma n_o r_o \int_1^{\infty} \left(\frac{r}{r_o}\right)^{-2} d\left(\frac{r}{r_o}\right) = \sigma n_o r_o \quad . \tag{I-2}$$

Thus, as the size of the hole decreases, the external collision rate decreases and the possibility of collisionless gas flow increases.

For example, for the largest hole used $r_o = 5 \times 10^{-3}$ cm, the pressure was 1 Torr, or $n_o = 3.6 \times 10^{16}/cm^3$, and the elastic cross

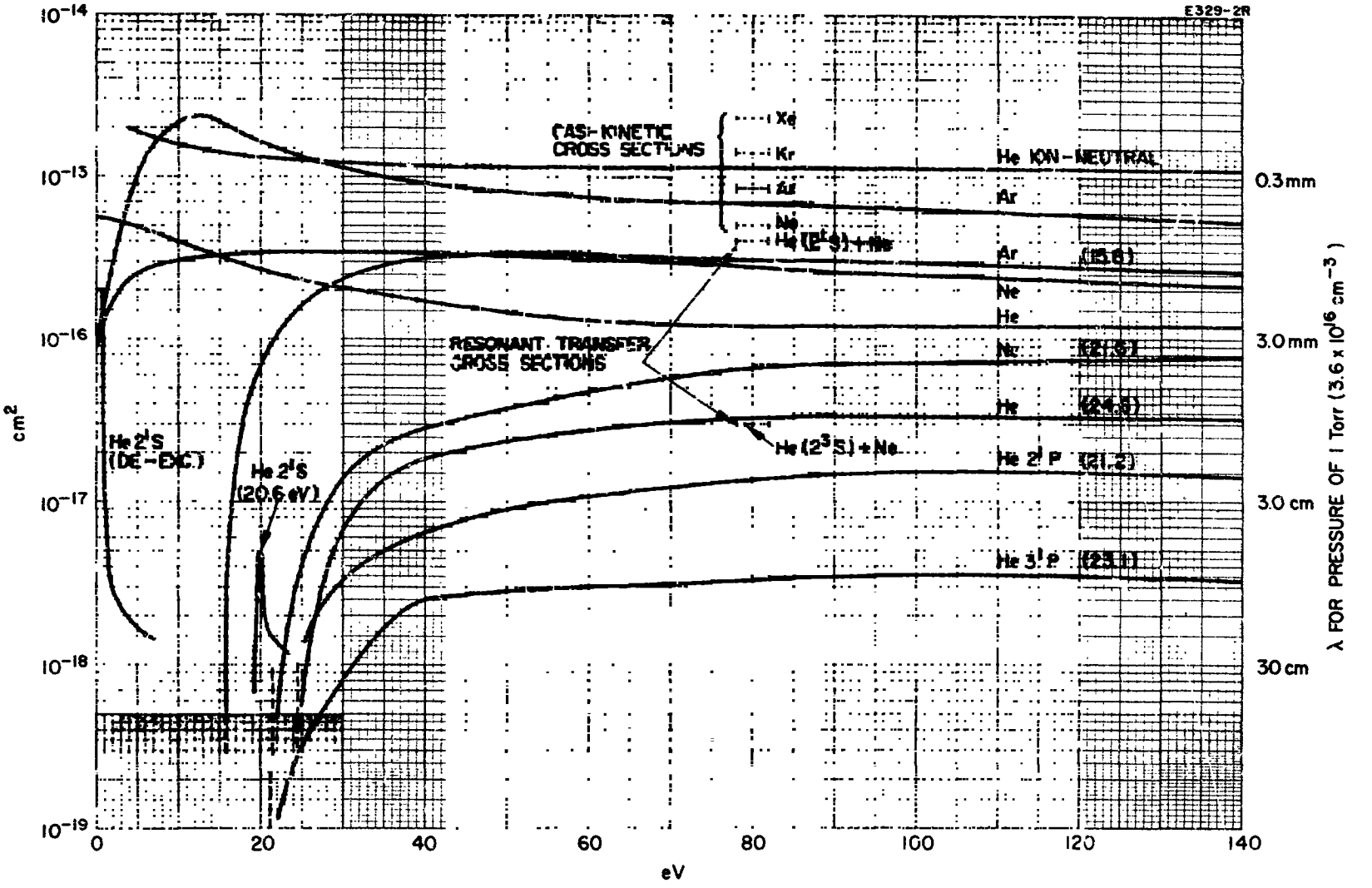

Fig. 30. Electron collision cross sections in argon, neon, and helium.

section with helium was $3 \times 10^{-16}/cm^2$. The electron collision probability is 0.053; the cross sections for inelastic collisions are less than one third of this value.

From (I-1) and (I-2) we also learn that it is not important to pump to a high ultimate vacuum, nor are obstructions to the flow important. If the obstructions have openings which are 10 to 100 times the hole diameter (several millimeters), the density drops sufficiently rapidly.

BLANK PAGE

APPENDIX II — CROSS SECTION DATA

The known cross sectional data on helium permit an evaluation of the sum of the integrals which appear in the second term of the exponent of eq. (11).

$$\sum_{\nu} \int_{\epsilon_\nu}^{\epsilon} \sigma_\nu (\epsilon') \, d\epsilon'$$

In Fig. 30 are plotted some important known cross sections on a logarithmic scale. The elastic cross sections,[33] ionization cross sections,[34] excitation cross section for the helium atom,[35] and the excitation cross section for the helium metastable singlet level[36] are taken from various sources. The ion-neutral cross section, which is dominated by charge transfer, is from Brown.[37] The deexcitation of the metastable helium atom by electrons is computed using the principle of detailed balancing. Also shown are the gas kinetic cross sections from Landolt-Börnstein[38] and those for resonant transfer of the metastable helium energy to the neon atom taken from Benton, et al.[39] The slopes with which the ionization cross sections rise at the threshold energy E_i are as follows: helium — 24.6 eV, 1.3×10^{-18} cm^2 (eV)$^{-1}$; neon — 21.6 eV, 1.5×10^{-18} cm^2 (eV)$^{-1}$; argon — 15.8 eV, 21×10^{-18} cm^2 (eV)$^{-1}$; krypton — 14.07 eV, 1200×10^{-18} cm^2 (eV)$^{-1}$.

In Fig. 31 we show the larger inelastic cross sections for helium on a linear scale from 0 to 70×10^{-18} cm^2. These collisions influence the shaping of the energy spectra. All excitation cross sections are summed and added to the ones for ionization, and the total sum is integrated. The integral

$$\int_0^{\epsilon} \sum_{\nu} \sigma_\nu (\epsilon') \, d\epsilon'$$

(a function of ϵ) is shown in two scales: the initial part up to 70×10^{-17} cm^2 eV and the main part up to 700×10^{-17} cm^2 eV. The integral initially rises quadratically, and at higher energies it rises more linearly.

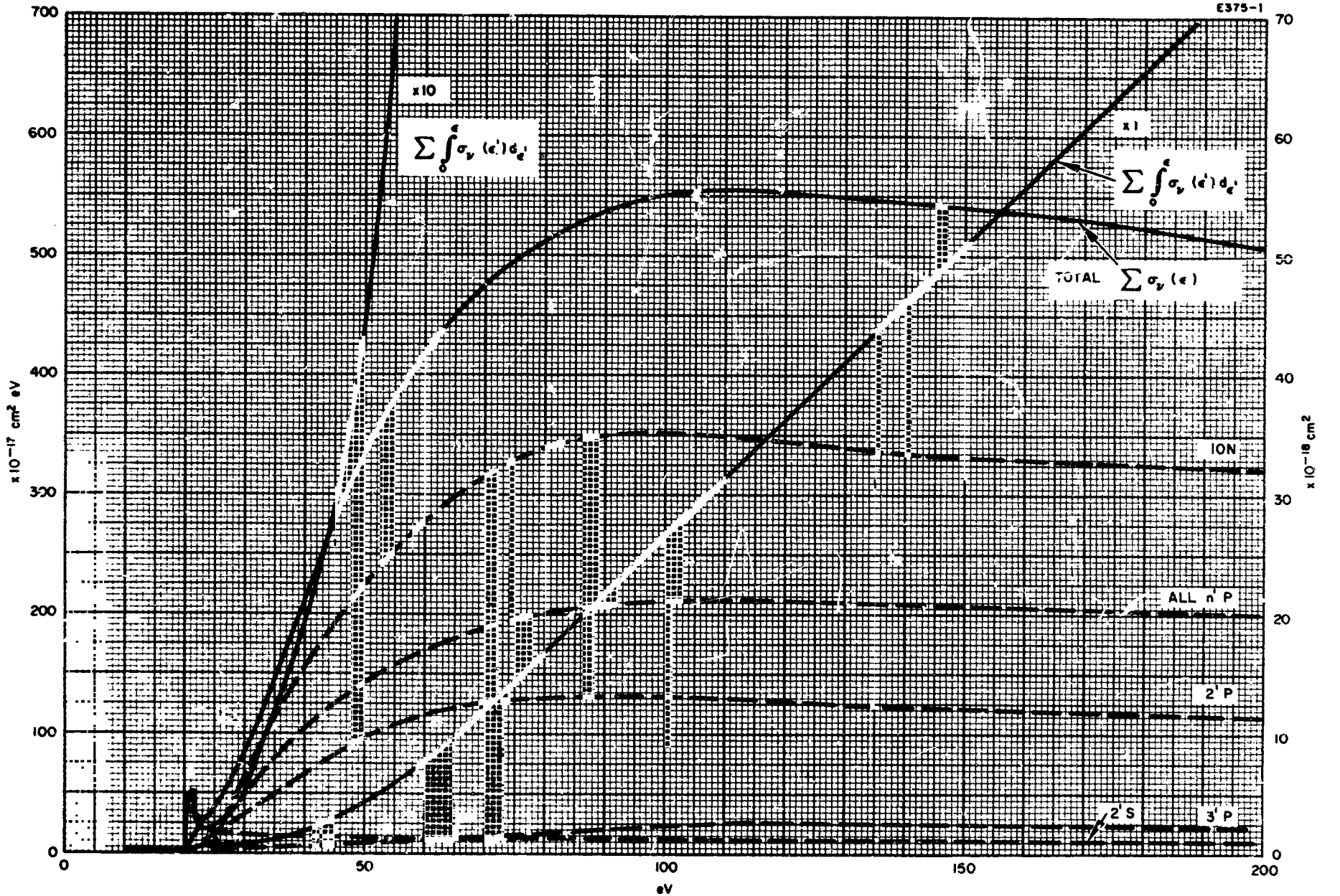

Fig. 31. Inelastic electron cross sections with helium.

REFERENCES

1. W. L. Faust, R. A. McFarlane, C. K. N. Patel, and C. G. B. Garrett, "Gas maser spectroscopy in the infrared," Appl. Phys. Letters, vol. 1, pp. 85-88; December, 1962. This was the first observation of high gain at 3.5 μ in xenon; however, no quantitative measurements were reported.

2. W. B. Bridges, "High optical gain at 3.5 μ in pure xenon," Appl. Phys. Letters, vol. 3, pp. 45-47; August 1963. This was the first published measurement of optical gain at 3.5 μ in pure xenon.

3. W. B. Bridges, and G. S. Picus, "Gas laser preamplifier performance," Appl. Optics, vol. 3, pp. 1189-1190; October, 1964.

4. R. A. Paananen and D. L. Bobroff, "Very high gain gaseous (Xe-He) optical maser at 3.5 μ," Appl. Phys. Letters, vol. 2, pp. 99-100; March, 1963.

5. W. B. Bridges, in "Receivers for Laser Radars," Technical Documentary Report No. RTD-TDR-63-4185 (Unclassified) (R. L. Forward, Ed.), p. 24; December, 1963.

6. E. I. Gordon, A. D. White, and J. D. Rigden, "Gain Saturation at 3.39 μ in the He-Ne Maser," Symposium on Optical Masers, Polytechnic Institute of Brooklyn, pp. 309-319; April, 1963.

7. W. W. Rigrod, "Gain saturation and output power of optical masers," J. Appl. Phys., vol. 34, pp. 2602-2609; September, 1963.

8. H. Heil and J. Y. Wada, "Electron energy spectra in gas laser devices," Hughes Research Laboratories Research Report No. 315; October 1964. Also see Section VI of this report.

9. E. I. Gordon and A. D. White, "Similarity laws for the effects of pressure and discharge diameter on gain of He-Ne lasers," Appl. Phys. Letters, vol. 3, pp. 199-201; December, 1963.

10. C. K. N. Patel, W. L. Faust, and R. A. McFarlane, "High gain gaseous (Xe-He) optical masers," Appl. Phys. Letters, vol. 1, pp. 84-85; December, 1962.

11. C. K. N. Patel, W. R. Bennett, Jr., W. L. Faust, and R. A. McFarlane, "Infrared spectroscopy using stimulated emission techniques," Phys. Rev. Letters, vol. 9, pp. 102-104; August, 1962.

12. W. R. Bennett, Jr., "Problems Related to High Power Gas Laser Systems," Institute for Defense Analyses Research Paper P-39, p. 30; July, 1963.

13. Y. M. Kagan, R. I. Lycgushchenko, and A. D. Khakhaev, "The excitation of inert gases in the positive column of a discharge at medium pressures," Opt. Spectr., vol. 14, pp. 317-322; 1963.

14. W. L. Faust, R. A. McFarlane, C. K. N. Patel, and C. G. B. Garrett, "Nobel gas optical maser lines at wavelengths between 2 and 35 μ," Phys. Rev., vol. 133, pp. A1476-A1486; 1964.

15. R. A. McFarlane, W. L. Faust, C. K. N. Patel, and C. G. B. Garrett, "Gas maser operation at wavelengths out to 28 μ," published in proceedings of the Paris Conference on Quantum Electronics, pp. 573-586; 1963.

16. W. T. Walter and S. M. Jarrett, "Strong 3.27 μ laser oscillation in xenon," Appl. Optics, vol. 3, pp. 789-790; June 1964.

17. H. Brunet and P. Laures, "New infrared gas laser transitions by removal of dominance," Phys. Letters, vol. 12, pp. 106-107; September 1964.

18. C. L. Tang, "Relative probabilities for the xenon laser transition," IEEE (Correspondence), vol. 51, pp. 219-220; January, 1963.

19. Raytheon Gaseous Laser Research Interim Engineering Report No. 2; October, 1964.

20. W. L. Faust and R. A. McFarlane, "Line strengths for noble gas maser transitions; calculations of gain/inversion at various wavelengths," J. Appl. Phys., vol. 35, pp. 2010-2015; July, 1964.

21. C. E. Moore, N. B. S. (U.S.) Circ. No. 467.

22. D. I. Mash, V. F. Papulvoskii, and L. P. Chirina, "On the operation of a xenon-krypton laser," Opt. Spectr., vol. 17, pp. 431-432; November, 1964.

23. For example, see J. D. Cobine, "Gaseous Conductors," Chapt. VIII, Dover Publications, Inc., New York.

24. For example, see J. R. Acton and J. D. Swift, "Cold Cathode Discharge Tubes," pp. 180-181, Academic Press, Inc., New York.

25. P. K. Tien, D. MacNair, and H. L. Hodges, "Electron beam excitation of gas laser transitions and measurements of cross sections of excitation," Phys. Rev. Letters, vol. 12, pp. 30-33; January, 1964.

26. See for example, H. Statz, C. L. Tang, and G. F. Koster, J. Appl. Phys., vol. 34, p. 2625; 1963.

27. S. C. Brown, "Basic Data of Plasma Physics," John Wiley and Sons, New York, p. 108; 1959.

28. F. W. Crawford, A. Garscadden, and R. S. Palmer, Proc. Sixth Int. Conf. on Ionization Phenomena in Gases, vol. 4, p. 53; 1953. J. D. Swift, Proc. Fifth Int. Conf. on Ionization Phenomena in Gases, vol. 3, p. 219; 1961. G. Medisuc, J. Appl. Phys., vol. 27, p. 1242; 1956, and "Probe Techniques for the Study of Plasma Phenomena," presented at Commission VII, URSI, Tokyo; 1963. S. Aisenberg, J. Appl. Phys., vol. 35, p. 130; 1964, and Appl. Phys. Letters, vol. 2, p. 187; 1963.

29. H. Heil, Proc. Sixth Int. Conf. on Ionization Phenomena in Gases, vol. 4, p. 71; 1963.

30. M. J. Druyvesteyn, Physica, vol. 3, p. 65; 1936. J. A. Smith, Physica, vol. 3, p. 543; 1936. M. J. Druyvesteyn and F. M. Penning, Rev. Mod. Phys., vol. 12, p. 87; 1940. W. P. Allis, Encycoped. Phys., vol. 21, p. 383; 1956.

31. H. Statz, C. L. Tang, and G. F. Koster, J. Appl. Phys., vol. 34, p. 2625; 1963, esp. Chap. IV, p. 2631.

32. E. I. Gordon, and A. D. White, Appl. Phys. Letters, vol. 3, p. 197, 199; 1963.

33. Landolt-Bornstein, "Zahlenwertz und Funktionen," 6th ed., Springer-Verlag, Berlin, vol. 1, Part 1, p. 327; 1950.

34. S. C. Brown, op. cit., pp. 108-111.

35. A. H. Gabriel and D. W. O. Heddle, Proc. Roy. Soc. (London), vol. A258, p. 124; 1960.

36. G. J. Schulz, Phys. Rev., vol. 116, p. 1141; 1959.

37. S. C. Brown, op. cit., p. 37.

38. Landolt-Börnstein, op. cit., p. 326 (from the self diffusion coefficient).

39. E. E. Benton, E. E. Ferguson, F. A. Matsen, and W. W. Robertson, Phys. Rev., vol. 128, p. 206; 1962.